

Probing flavor constrained SMEFT operators through tc production at the Muon collider

Subhaditya Bhattacharya, Sahabub Jahedi, Soumitra Nandi, and Abhik Sarkar

Department of Physics, Indian Institute of Technology, Guwahati, Assam 781039, India

E-mail: subhab@iitg.ac.in, sahabub@iitg.ac.in,

soumitra.nandi@iitg.ac.in, sarkar.abhik@iitg.ac.in

ABSTRACT: We investigate flavor violating four-Fermi Standard Model Effective Field Theory (SMEFT) operators of dimension-six that can be probed via tc ($\bar{t}c + t\bar{c}$) production at the multi-TeV muon collider. We study different FCNC and FCCC processes related to B , B_s , K and D decays and mixings, sensitive to these operators and constrain the corresponding couplings. The tensor operator turns out to be most tightly bound. We perform event simulation of the final state signal from tc production together with the SM background to show that operators after flavor constraint can reach the discovery limit at 10 TeV muon collider. We further adopt the optimal observable technique (OOT) to determine the optimal statistical sensitivity of the Wilson coefficients and compare them with the flavor constraints. We use the limits to predict the observational sensitivities of the rare processes like $K_L \rightarrow \pi_0 \ell \ell$, $D_0 \rightarrow \mu \mu$, $t \rightarrow c \ell \ell$.

KEYWORDS: Specific BSM Phenomenology, SMEFT, Top FCNC

Contents

1	Introduction	1
2	Phenomenological framework	3
3	Flavor constraints and predictions	5
3.1	Flavor and top-quark constraints	5
3.2	Prediction on different observables	12
4	Collider analysis	17
4.1	tc ($\bar{t}c + t\bar{c}$) production cross-section	17
4.2	Signal and background processes	19
4.2.1	Event simulation	19
4.3	Cut based Analysis	20
5	Optimal Observable Technique	21
5.1	OOT Sensitivities	22
6	Sensitivity of "flavor-relaxed" ($C_{lequ}^{(1)32}/\Lambda^2$) at the 500 GeV ILC	26
7	Summary and Conclusion	28
A	Loop function for $B_q - \bar{B}_q$ mixings and amplitudes of $t \rightarrow b\ell\nu$	29
B	Renormalization Group (RG) Equations	29

1 Introduction

Search for physics beyond the Standard Model (BSM) at the Large Hadron Collider (LHC) and preceding experiments has not provided a conclusive result yet despite extensive search and data analysis. This suggests that BSM physics is either weakly coupled, or exists at energy scales considerably removed from the electroweak scale, or possesses signals unaccounted from the standard searches done so far, or all of them. Therefore exploring BSM physics via Standard Model Effective Field Theory (SMEFT) has gained considerable attention in recent times. The construction of effective theory assumes the knowledge of only low scale theory (SM here), so that the Lagrangian involving higher dimensional operators can be written as [1–3]:

$$\mathcal{L} = \mathcal{L}_{SM} + \sum_{n=5}^{\infty} \frac{1}{\Lambda^{n-4}} \sum_i C_i \mathcal{O}_i^n, \quad (1.1)$$

where \mathcal{O}_i 's are the effective operators constructed out of the Standard Model (SM) fields respecting the SM gauge symmetry, C_i 's are the new physics (NP) couplings or Wilson coefficients (WCs), through which the effect of BSM scenarios can be realised. Λ denotes the NP scales integrated out, which has power $(n - 4)$ depending on the mass dimension n of the operator \mathcal{O}_i under consideration. SMEFT has been studied extensively via operators of dimension-five [1], six [2, 3], seven [4, 5], and eight [6, 7] to estimate NP deviations in a model-independent way. In this study, we will use the dimension-six SMEFT operators that contribute to $t\bar{c}$ ($\bar{t}c + t\bar{c}$) production at collider¹ after taking the flavor constraints into account.

As we know that the renormalization-group equations (RGE) allow one to compute the running and mixing between the BSM scale down to the electroweak scale and further down to the scale of low-energy precision experiments, the SMEFT can be matched to a low energy EFT. It could be done following a two step matching procedure. The coefficients C_i 's generated at the scale Λ will be related to their values at the electroweak scale $v \sim 246$ GeV, and these coefficients can further be related to the WCs of a low-energy EFT through RGE running. Therefore, any constraints obtained on the WCs from low energy data will in turn limit $C_i(\Lambda)$'s at any given BSM scale Λ . The flavor changing neutral current (FCNC) processes are loop suppressed in the SM, and any tree level NP contributions to such processes will have limited parameter spaces allowed by the data. Similarly, the availability of precise data on the flavor changing charged current (FCCC) processes at the low energy could play an essential role to constrain the NP parameter space contributing to such processes at the tree level. Therefore, study of the FCNC and FCCC processes at the low energy will play a crucial role in exploring flavor violating NP effects under the SMEFT framework.

FCNC processes such as $b \rightarrow s(d)$ transitions are one of the most important probes in this connection, as there is no such interactions within the SM at the tree level². Such flavor observables therefore provide an important bound on the corresponding SMEFT operators, see for example, [11–16]. In this study, we focus on the observables related to the semi leptonic and leptonic decays of B , B_s , K mesons via the processes $b \rightarrow s(d)\ell^+\ell^-$ and $s \rightarrow d\ell^+\ell^-$ where the data is available only for $\ell = \mu$ or e . In addition, we have considered the available data on $B - \bar{B}$ and $B_s - \bar{B}_s$ mixing amplitudes to constrain the NP parameter spaces. Among the FCCC processes, we mainly consider the available data on semi leptonic and leptonic decays of B , K , D and D_s mesons via $b \rightarrow c(u)\ell^+\bar{\nu}$, $s \rightarrow u\ell^+\bar{\nu}$ and $c \rightarrow d(s)\ell^+\bar{\nu}$ transitions, respectively.

Along with flavor observables, top-quark physics also plays an important role under SMEFT framework as it has $O(1)$ Yukawa coupling, which is crucial to explain the origin of electroweak symmetry breaking (EWSB). Several analyses under SMEFT framework in the top-quark sector have been performed in [17–19]. This motivates us to choose $\bar{t}c(t\bar{c})$ production

¹Understandably the contributions from dimension-eight operators will be diminished by powers of Λ^2 and the effect will be milder, unless some specific assumption on NP is taken into account.

²Higher order corrections to $b \rightarrow s(d)$ transitions have been studied in [8–10].

as an example process to study.

The stringent constraint on the dimension-six effective operators derived from the flavor observables indicate that their production at the LHC is small, while the SM background is huge and mostly irreducible, so that a prediction requires thorough analysis. If we choose the conservative limits, it is also difficult to probe them in a future electron-positron collider with a maximum centre-of-mass (CM) energy of 3 TeV. Therefore we examine the process at high energy muon collider [20]. Muons, being fundamental particles, provide the advantage of directing their entire energy towards short-distance scattering rather than having it distributed among the partons. As a result, a 14 TeV muon collider can exhibit effectiveness on par with a 100 TeV proton-proton collider [21]. This high-energy capability is particularly advantageous for both the exploration of new heavy particles along with indirect measurements at elevated energy levels. Hence, a multi-TeV muon collider acts as both discovery and precision machine altogether. Limited studies on tc production at lepton colliders have been documented in the existing literature [22–25]. In a somewhat similar analysis [25], the flavor constraints are obtained from rare B decay processes, applicable to the vector operators only, while ours is done considering all possible flavor observables applicable to all of the vector, scalar and tensor type four-Fermi operators.

Further, we study the optimal statistical precision of the NP couplings using the optimal observable technique (OOT) [26–29]. OOT has been widely employed for precision analysis in various domains, including Higgs couplings at e^+e^- colliders [30, 31], top-quark properties at the $\gamma\gamma$ colliders [32–34] and e^+e^- colliders [35], CP properties of the Higgs at the LHC [36], $e\gamma$ colliders [37], and muon collider [38]. Some recent works involving estimation of Z -couplings with heavy charged fermion [39] and anomalous neutral triple gauge couplings [40, 41] are also explored using the OOT.

The paper is arranged in the following way. In Section 2, we discuss the relevant phenomenological framework for our analysis. Then in Section 3, we study the constraints from flavor physics, followed by collider simulation at $\mu^+\mu^-$ collider in Section 4. Section 5 elaborates OOT framework and the optimal limits on flavor violating dimension-six effective couplings. In Section 6, we discuss the collider probe of scalar operator contributing to $3 \rightarrow 2$ (hadronic) transition at e^+e^- machine. Finally, we summarize our conclusion in Section 7.

2 Phenomenological framework

Our goal of the analysis is to probe the dimension-six flavor violating effective (EFT) operators that contributes to tc ($\bar{t}c + t\bar{c}$) production at the future muon collider. The Feynman graphs for the $t\bar{c}$ production are shown in figure 1 ($\bar{t}c$ graphs are similar with same contributions and not shown here). There are essentially two different contributions: (i) via Ztc vertex and (ii) four-Fermi $\mu\mu tc$ contact interaction. As elaborated later, operators contributing to Ztc affect the process very mildly, while the main contribution arises from the four-Fermi operators.

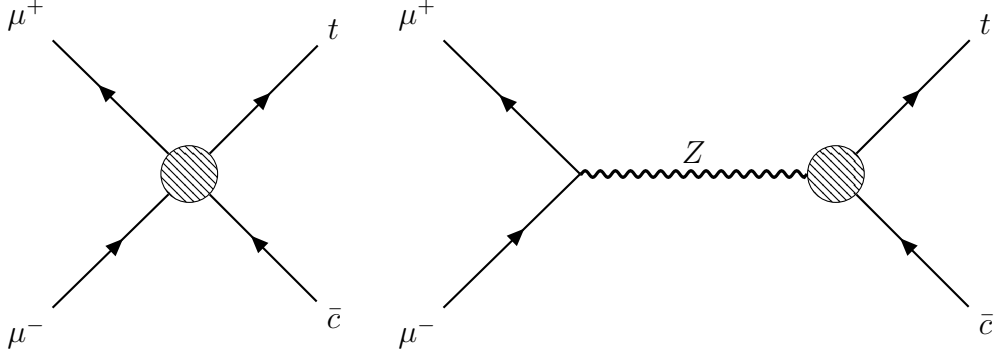


Figure 1: Feynman diagrams that induce $t \bar{c}$ production at the muon collider; left: effective four-Fermi ($\mu\mu tc$) couplings, right: effective Ztc couplings. The conjugate processes look alike with exactly same cross-section.

There are three types of four-Fermi operators containing i) four leptons, ii) four quarks and iii) two leptons and two quarks, where the last one serves our purpose. There are seven operators that contribute to the $\mu^+\mu^- \rightarrow tc$ production, as given by [3, 24],

$$\begin{aligned}
\mathcal{O}_{lq}^{(1)} &= (\bar{l}_p \gamma^\mu l_r)(\bar{q}_i \gamma_\mu q_j), \\
\mathcal{O}_{lq}^{(3)} &= (\bar{l}_p \gamma^\mu \tau^I l_r)(\bar{q}_i \gamma_\mu \tau^I q_j), \\
\mathcal{O}_{eu} &= (\bar{e}_p \gamma^\mu e_r)(\bar{u}_i \gamma_\mu u_j), \\
\mathcal{O}_{lu} &= (\bar{l}_p \gamma^\mu l_r)(\bar{u}_i \gamma_\mu u_j), \\
\mathcal{O}_{qe} &= (\bar{q}_p \gamma^\mu q_r)(\bar{e}_i \gamma_\mu e_j), \\
\mathcal{O}_{lequ}^{(1)} &= (\bar{l}_p^a e_r) \epsilon_{ab} (\bar{q}_i^b u_j), \\
\mathcal{O}_{lequ}^{(3)} &= (\bar{l}_p^a \sigma^{\mu\nu} e_r) \epsilon_{ab} (\bar{q}_i^b \sigma_{\mu\nu} u_j),
\end{aligned} \tag{2.1}$$

where l (e) is the left (right)-handed lepton doublet (singlet), q is the left-handed quark doublet, and u (d) is the up (down)-type right-handed quark singlets. Apart, p, r, i, j indicates flavor indices, τ^I are the Pauli matrices, $\epsilon = -i\tau_2$, $\sigma^{\mu\nu} = \frac{i}{2}[\gamma^\mu, \gamma^\nu]$. Using Eq. (2.1), the most general four-Fermi effective Lagrangian for $\mu\mu tc$ contact interaction can be written as,

$$\mathcal{L}_{\mu\mu tc} = \frac{1}{\Lambda^2} \sum_{s,t=L,R} [\mathcal{V}_{st}(\bar{\mu}\gamma_\mu P_s \mu)(\bar{t}\gamma^\mu P_t c) + \mathcal{S}_{st}(\bar{\mu} P_s \mu)(\bar{t} P_t c) + \mathcal{T}_{st}(\bar{\mu}\sigma_{\mu\nu} P_s \mu)(\bar{t}\sigma^{\mu\nu} P_t c)], \tag{2.2}$$

where vector-like (\mathcal{V}_{st}), scalar-like (\mathcal{S}_{st}) and tensor-like (\mathcal{T}_{st}) couplings can be expressed in

terms of the WCs of the seven four-Fermi operators as in Eq. (2.1) as,

$$\begin{aligned}\mathcal{V}_{LL} &= (C_{lq}^{(1)ij} - C_{lq}^{(3)ij}), \quad \mathcal{V}_{LR} = C_{lu}^{ij}, \quad \mathcal{V}_{RR} = C_{eu}^{ij}, \quad \mathcal{V}_{RL} = C_{qe}^{ij}, \\ \mathcal{S}_{RR} &= -C_{lequ}^{(1)ij}, \quad \mathcal{S}_{LL} = \mathcal{S}_{LR} = \mathcal{S}_{RL} = 0, \\ \mathcal{T}_{RR} &= -C_{lequ}^{(3)ij}, \quad \mathcal{T}_{LL} = \mathcal{T}_{LR} = \mathcal{T}_{RL} = 0.\end{aligned}\tag{2.3}$$

Note that for vector operators we have all the helicity combination of fermions appear for both lepton and quarks, while for the scalar and tensor couplings only RR combination is non zero. In Eq. (2.2), the \mathcal{S}_{LL} and \mathcal{T}_{LL} also get a matching condition from the hermitian conjugate SMEFT operators, leading to $-C_{lequ}^{(1)ji*}$ and $-C_{lequ}^{(3)ji*}$, respectively. The above parametrization will be used for the collider simulation later.

The tree-level dimension-six EFT operators that contribute to effective Ztc vertex are,

$$\begin{aligned}\mathcal{O}_{\phi q}^{(1)} &= i(\phi^\dagger D^\mu \phi)(\bar{q}_i \gamma_\mu q_j), \\ \mathcal{O}_{\phi q}^{(3)} &= i(\phi^\dagger D^\mu \tau^I \phi)(\bar{q}_i \gamma_\mu \tau^I q_j), \\ \mathcal{O}_{\phi u} &= i(\phi^\dagger D^\mu \phi)(\bar{u}_i \gamma_\mu u_j).\end{aligned}\tag{2.4}$$

Therefore, the effective Lagrangian containing Ztc vertex³ is,

$$\mathcal{L}_{Ztc} = g \frac{v^2}{\Lambda^2} \bar{t} \gamma^\mu (a_L^Z P_L + a_R^Z P_R) c Z_\mu,\tag{2.5}$$

where, $P_{L(R)} = \frac{1-(+)\gamma^5}{2}$, a_L and a_R are the functions of $C_{\phi q}^{(1)ij}$, $C_{\phi q}^{(3)ij}$ and $C_{\phi u}^{ij}$ as,

$$a_L^Z = \frac{1}{4c_w} (C_{\phi q}^{(1)ij} - C_{\phi q}^{(3)ij}), \quad a_R^Z = \frac{1}{4c_w} C_{\phi u}^{ij};\tag{2.6}$$

where, $c_w = \cos \theta_w$, θ_w is weak mixing angle.

3 Flavor constraints and predictions

In this section, we study all possible flavor and top quark related experimental constraints that put bound on the dimension-six effective couplings of our interest as described above. We then make some observable predictions for some rare processes based on the constraints obtained for the effective operators.

3.1 Flavor and top-quark constraints

Note that the operators defined in Eq. (2.1) will contribute to various low energy observables related to the FCNC and FCCC processes. In the following we will discuss different inputs which we have considered in this analysis.

³ γtc vertex is forbidden by $U(1)$ gauge invariance.

FCNC processes: Most important constraints will be obtained from the semileptonic and leptonic decays of via $b \rightarrow s\ell^+\ell^-$ decays. The corresponding low energy effective Hamiltonian is given by [42, 43]

$$\mathcal{H}_{\text{eff}} = \mathcal{H}_{\text{eff}}^{\text{SM}} - \frac{4G_F}{\sqrt{2}} \lambda_t^{bs} \frac{e_0^2}{16\pi^2} \left(\Delta C_9^\ell O_9^\ell + \Delta C_{10}^\ell O_{10}^\ell + C_9^{\prime\ell} O_9^{\prime\ell} + C_{10}^{\prime\ell} O_{10}^{\prime\ell} + C_S^\ell O_S^\ell + C_P^\ell O_P^\ell \right. \\ \left. + C_S^{\prime\ell} O_S^{\prime\ell} + C_P^{\prime\ell} O_P^{\prime\ell} \right), \quad (3.1)$$

where ℓ stands here for all the three lepton fields: e, μ and τ . Here, e_0 and G_F are the $U(1)_{em}$ and Fermi coupling constants, $\lambda_t^{bs} = V_{tb}V_{ts}^*$ is the CKM combination. The four-Fermi operators as in Eq. (3.1) are expressed as,

$$O_9^\ell = (\bar{s}\gamma_\mu P_L b)(\bar{\ell}\gamma^\mu \ell), \quad O_S^\ell = (\bar{s}P_R b)(\bar{\ell}\ell), \\ O_{10}^\ell = (\bar{s}\gamma_\mu P_L b)(\bar{\ell}\gamma^\mu \gamma^5 \ell), \quad O_P^\ell = (\bar{s}P_R b)(\bar{\ell}\gamma^5 \ell). \quad (3.2)$$

The O' operators can be obtained by interchanging $\{L \leftrightarrow R\}$ from the operators O as above in Eq. (3.2). The SM Hamiltonian (\mathcal{H}^{SM}) already incorporates O_9^ℓ and O_{10}^ℓ operators with WCs C_9^{SM} and C_{10}^{SM} . Therefore, ΔC_9^ℓ and ΔC_{10}^ℓ denote the WCs corresponding to O_9^ℓ and O_{10}^ℓ operators stemming from NP. Remaining effective operators are absent in the SM framework thus comes purely from NP contribution. We will use Eq. (3.1) and Eq. (3.2) to obtain limits from $b \rightarrow s$ and $b \rightarrow d$ transitions and translate them in terms of the WCs of our notation as in Eq. (2.1). Following a tree level matching procedure, one can express the WCs defined in Eq. (2.1) in terms of the WCs of in the low energy effective Hamiltonian given above [44].

- $b \rightarrow s\mu\mu$ decay: $b \rightarrow s$ transitions are absent at the tree level within the SM; therefore observables having such transitions provide intriguing indications of potential NP effects through ΔC_9^μ and ΔC_{10}^μ [45–49]. They stem from several experimental observations like $B \rightarrow K\mu\mu$, $B \rightarrow K^*\mu\mu$, and $B_s \rightarrow \phi\mu\mu$, which have been considered in this analysis [50–59]. The latest experimental results from the LHCb on lepton flavor universality (LFU) ratio R_K and R_K^* [60, 61] are in great agreement with the SM prediction which indicates a tighter constraint on ΔC_9^μ and ΔC_{10}^μ . After matching dimension-six effective couplings in Eq. (2.1) with the Hamiltonian written in Eq. (3.1), we get [44],

$$\Delta C_9^\mu = \left(\frac{\alpha}{\lambda_t^{bs}\pi} \right) \left(\frac{v^2}{\Lambda^2} \right) \left(C_{lq}^{(1)32} + C_{lq}^{(3)32} + C_{qe}^{32} \right), \\ \Delta C_{10}^\mu = \left(\frac{\alpha}{\lambda_t^{bs}\pi} \right) \left(\frac{v^2}{\Lambda^2} \right) \left(C_{lq}^{(1)32} - C_{lq}^{(3)32} - C_{qe}^{32} \right), \quad (3.3)$$

where $\alpha = e_0^2/4\pi$ is fine-structure constant and v is the vacuum expectation value (vev) of the SM Higgs. We can see that $\mathcal{O}_{lq}^{(1)}$, $\mathcal{O}_{lq}^{(3)}$, and \mathcal{O}_{qe} are the three dimension-six SMEFT operators that contribute to $b \rightarrow s\mu\mu$ transition. Since we have analyzed the constraints by choosing one operator at a time, therefore, for \mathcal{O}_{qe} and $\mathcal{O}_{lq}^{(3)}$ operators, $\Delta C_9^\ell = -\Delta C_{10}^\ell$; whereas for $\mathcal{O}_{lq}^{(1)}$, we have $\Delta C_9^\ell = \Delta C_{10}^\ell$. Following the analysis

discussed in [49], we obtain $\Delta C_9^\mu = -0.23$ and transmitting this limit to couplings of dimension-six SMEFT operator using Eq. (3.3), the constraints are noted in Table 1.

- $b \rightarrow d\mu\mu$ decay: $b \rightarrow d\mu\mu$ transition is another FCNC process which also plays an important role to constrain NP scenarios [62, 63]. Like $b \rightarrow s\mu\mu$ transition, here also $\mathcal{O}_{lq}^{(1)}$, $\mathcal{O}_{lq}^{(3)}$, and \mathcal{O}_{qe} operators contribute. Consequently, relations between the WCs in two different parametrizations are similar to that in Eq. (3.3), just with a trivial substitution of $\lambda_t^{bd} = V_{tb}^* V_{td}$ and appropriate indices on WCs. We utilize the experimentally determined value of $\Delta C_9^\mu = -0.53$ from the global fits of $B^+ \rightarrow \pi^+ \mu^+ \mu^-$, $B_s^0 \rightarrow \bar{K}^{*0} \mu^+ \mu^-$, $B^0 \rightarrow \mu^+ \mu^-$, and radiative $B \rightarrow X_d \gamma$ decays data sourced from [63], to relate the dimension-six effective couplings of our choice (Eq. (3.3)). The constraints from this decay channel for these three dimension-six effective couplings are tabulated in Table 1.
- $K_L \rightarrow \mu\mu$ decay: The expression for the branching ratio of $K_L \rightarrow \mu^+ \mu^-$ decay using the Hamiltonian in Eq. (3.1) can be expressed as [64, 65],

$$\text{BR}(K_L \rightarrow \mu^+ \mu^-) = \frac{\tau_L f_K^2 m_K^3 \beta_\mu}{16\pi} \left| N_L^{LD} - \left(\frac{2m_\mu}{m_K} \right) \frac{G_F \alpha}{\sqrt{2}\pi} \text{Re} \left[-\lambda_c^{sd} \frac{Y_c}{s_W^2} + \lambda_t^{sd} C_{10}^\mu \right] \right|^2. \quad (3.4)$$

In the above Eq. (3.4), τ_L represents the mean life of the K_L meson, m_μ and m_K denote the masses of the muon and kaon respectively, G_F stands for the Fermi constant, and β_μ and λ_q^{sd} are defined as:

$$\beta_\mu = \sqrt{1 - \frac{4m_\mu^2}{m_K^2}}, \quad \lambda_q^{sd} = V_{qd}^* V_{qs}. \quad (3.5)$$

Y_c indicate short-distance contribution from SM while $N_L^{LD} = \pm[0.54(77) - 3.95i] \times 10^{-11}$ in GeV^{-2} is the long-distance contribution [66, 67] and $C_{10} = C_{10}^{\text{SM}} + \Delta C_{10}^\mu$. The relevant operators are $\mathcal{O}_{lq}^{(1)}$, $\mathcal{O}_{lq}^{(3)}$ and \mathcal{O}_{qe} that contribute to this observables. ΔC_{10}^μ respects Eq. (3.3). Resulting limits on dimension-six effective couplings are written in Table 1.

- $B_q - \bar{B}_q$ mixing (with $q = d, s$): B^0 or B_s mesons exhibit oscillatory behaviour between particle and antiparticle states, a phenomenon arising from the influence of flavor-changing weak interactions. These meson-antimeson mixings are the $\Delta B = 2$ FCNC processes. In presence of NP, the mixing amplitude or the frequency of meson-antimeson oscillations is defined as,

$$\Delta M_q = 2|M_{12}^q| = 2|M_{12}^{q,SM} + M_{12}^{q,NP}|, \quad (3.6)$$

with

$$M_{12}^q = \frac{\langle B_q | \mathcal{H}_{eff}^{\Delta B=2} | \bar{B}_q \rangle}{2M_{B_q}}. \quad (3.7)$$

The dominant contribution to $M_{12}^{q,SM}$ in the SM arises from the top mediated box diagrams [68–70], and the corresponding contribution is given by,

$$M_{12}^{q,SM} = \frac{G_F^2}{24\pi^2} m_{B_q} f_{B_q}^2 \hat{B}_q \eta_B f(x^2) (\lambda_t^{bq})^2. \quad (3.8)$$

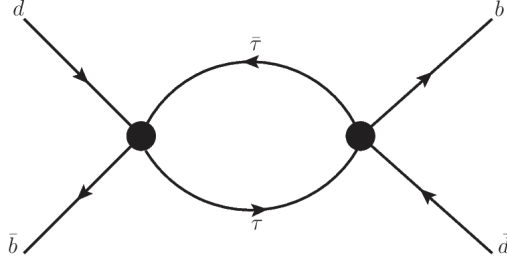


Figure 2: τ mediated 1-loop NP contribution to $\Delta m_{B_d^0}$.

Here, $m_{B_d}(m_{B_s})$ and $f_{B_{d(s)}^0} = 190.0$ (230.3) MeV are the masses and decay constants, $\hat{B}_{d(s)} = 1.222$ (1.232) is the bag factor of $B_{d(s)}^0$ meson respectively, $\eta_B = 0.55$ is the QCD correlation factor [71], and $\lambda_t^{bd(s)} = V_{tb}V_{td(s)}^*$. The Inami-Lim function $f(x)$ is given by [72],

$$f(x) = x \left(\frac{1}{4} + \frac{9}{4(1-x)} - \frac{3}{2(1-x)^2} \right) - \frac{3x^3 \log x}{(1-x)^3}, \quad x = \frac{m_t}{m_W}. \quad (3.9)$$

We already mentioned that the SMEFT operators in Eq. (2.1) contribute to the FCNC processes like $b \rightarrow s\mu^+\mu^-$ and $b \rightarrow d\mu^+\mu^-$. The four-Fermi operators in Eqs. (3.1) and (3.2), may contribute to $B_s - \bar{B}_s$ and $B^0 - \bar{B}^0$ mixing amplitudes respectively via the diagram shown in figure 2. In our scenario, the dispersive part of the diagram in figure 2 will contribute to M_{12}^q . The dominant contribution will arise from a τ mediated loop via the insertion of operators \mathcal{O}_9 and \mathcal{O}_{10} . From the dispersive part of the diagram in figure 2, we obtain,

$$\begin{aligned} M_{12}^{q, NP} = & -\frac{G_F^2 \alpha^2}{8\pi^2} m_{B_i} f_{B_i}^2 \hat{B}_i \eta_B (\lambda_t^{bq})^2 \left[4 \left((\Delta C_9^2 + \Delta C_{10}^2) m_b^2 + 4\Delta C_{10}^2 m_\tau^2 \right) \log \frac{\Lambda^2}{m_\tau^2} \right. \\ & + (2m_b^2 (\Delta C_9^2 + \Delta C_{10}^2) + m_\tau^2 (3\Delta C_{10}^2 - \Delta C_9^2)) \text{DiscB}[2m_b^2, m_\tau, m_\tau] \\ & \left. + 4(\Delta C_9^2 + \Delta C_{10}^2) m_b^2 - 2m_\tau^2 (\Delta C_9^2 - 7\Delta C_{10}^2) \right]. \end{aligned} \quad (3.10)$$

The expression of $\text{DisB}[\mathbf{a}, \mathbf{b}, \mathbf{c}]$ function in the above equation is written in the appendix. As we have discussed earlier, the contributions to $b \rightarrow s\tau^+\tau^-$ will come from $\mathcal{O}_{lq}^{(1)}$, $\mathcal{O}_{lq}^{(3)}$ and \mathcal{O}_{qe} . The amplitude is calculated using the Hamiltonian described in Eq. (3.1). Therefore, effective couplings related to these operators obey Eq. (3.3). The relevant constraints from this observable are presented in Table 1.

- $B_s^0 \rightarrow \mu\mu$ decay: Following Eq. (3.1), the branching ratio of $B_s^0 \rightarrow \mu^+\mu^-$ turns out [73],

$$\text{BR}(B_s^0 \rightarrow \mu^+\mu^-) = \tau_{B_s} \frac{G_F^2 \alpha^2 M_{B_s} f_{B_s}^2 m_\mu^2 (\lambda_t^{bs})^2}{16\pi^3} \sqrt{1 - \frac{4m_\mu^2}{M_{B_s}^2}} |C_{10}^\mu|^2. \quad (3.11)$$

The branching ratio of this rare decay is $(2.69^{+0.37}_{-0.35}) \times 10^{-9}$ [71, 74]. Understandably, $\mathcal{O}_{lq}^{(1)}$, $\mathcal{O}_{lq}^{(3)}$, and \mathcal{O}_{qe} contribute to this branching ratio. Using Eq. (3.3), the constraints obtained on the effective couplings for the relevant operators are tabulated in Table 1.

- $K^\pm \rightarrow \pi^\pm \nu \nu$ decay: The effective Hamiltonian relevant to $s \rightarrow d$ transitions is parameterized as [75, 76],

$$\mathcal{H}_{\text{eff}}^{s \rightarrow d} = \frac{G_F}{\sqrt{2}} \lambda_t^{sd} \left(\sum_{i=1}^{10} C_i O_i + \sum_{\ell=e,\mu,\tau} C_{\nu_\ell}^L O_{\nu_\ell}^L \right), \quad (3.12)$$

where $\lambda_t^{sd} = V_{ts} V_{td}^*$. The details of $O_1 - O_{10}$ operators are discussed in [75]. The operator relevant to $K^\pm \rightarrow \pi^\pm \nu \nu$ decay is

$$\begin{aligned} O_{\nu_\ell}^L &= \alpha (\bar{d} \gamma^\mu (1 - \gamma^5) s) (\bar{\nu}_\ell \gamma_\mu (1 - \gamma^5) \nu_\ell), \\ O_{\nu_\ell}^R &= \alpha (\bar{d} \gamma^\mu (1 + \gamma^5) s) (\bar{\nu}_\ell \gamma_\mu (1 - \gamma^5) \nu_\ell). \end{aligned} \quad (3.13)$$

The WC is $C_{\nu_\ell}^L = C_{\nu_\ell}^{L,\text{SM}} + \delta C_{\nu_\ell}^L$ with SM contribution

$$C_{\nu_\ell}^{L,\text{SM}} = \frac{1}{2\pi s_w^2} \left(\frac{\lambda_c^{sd}}{\lambda_t^{sd}} X_c^\ell + X_t \right), \quad (3.14)$$

where $X_t = 1.48$ is the short-distance NLO QCD correction arises from top-quark, $X_c^e \simeq X_c^\mu = 1.04 \times 10^{-3}$ and $X_c^\tau = 0.70 \times 10^{-3}$ are the short-distance charm contribution with the NLO logarithmic approximation [76, 77]. By correlating the dimension-six effective operators from Eq. (2.1) with those specified in Eq. (3.14), we can express the dimension-six effective couplings [78] as,

$$\delta C_{\nu_\ell}^L = \frac{2\pi}{e_0^2 \lambda_t^{sd}} \frac{v^2}{\Lambda^2} \left[C_{lq}^{(1)21} - C_{lq}^{(3)21} \right], \quad \delta C_{\nu_\ell}^R = 0. \quad (3.15)$$

The branching ratio of $B^+ \rightarrow \pi^+ \nu \nu$ decay is expressed as [78, 79],

$$\mathcal{B}(K^+ \rightarrow \pi^+ \nu \bar{\nu}) = \frac{2\alpha^2 |\lambda_t^{sd}|^2 \mathcal{B}(K^+ \rightarrow \pi^0 e^+ \nu_e)}{|V_{us}|^2} \sum_{\ell=e,\mu,\tau} |C_{\nu_\ell}^L + C_{\nu_\ell}^R|^2. \quad (3.16)$$

We take $\mathcal{B}(K^+ \rightarrow \pi^0 e^+ \nu_e) = (5.07 \pm 0.04) \times 10^{-2}$ and $\mathcal{B}(K^+ \rightarrow \pi^+ \nu \nu) = (1.14^{+0.40}_{-0.33}) \times 10^{-10}$ from the PDG average [80], and obtain $\delta C_{\nu_\ell} = -3.31$. Following Eq. (3.14), constraints on dimension-six effective couplings are noted in Table 1.

FCCC processes:

- $b \rightarrow q \ell \nu_\ell$ decay: The most general effective Hamiltonian for $b \rightarrow c(u) \ell \nu_\ell$ transitions is written as [82],

$$\mathcal{H}_{\text{eff}}^{b \rightarrow q \ell \bar{\nu}_\ell} = \frac{4G_F}{\sqrt{2}} V_{qb} [(1 + C_{V_1}^\ell) \mathcal{O}_{V_1}^\ell + C_{V_2}^\ell \mathcal{O}_{V_2}^\ell + C_{S_1}^\ell \mathcal{O}_{S_1}^\ell + C_{S_2}^\ell \mathcal{O}_{S_2}^\ell + C_T^\ell \mathcal{O}_T^\ell], \quad (3.17)$$

with the operators

$$\begin{aligned}
\mathcal{O}_{V_1}^\ell &= (\bar{q}_L \gamma^\mu b_L)(\bar{\ell}_L \gamma_\mu \nu_{\ell L}), \\
\mathcal{O}_{V_2}^\ell &= (\bar{q}_R \gamma^\mu b_R)(\bar{\ell}_L \gamma_\mu \nu_{\ell L}), \\
\mathcal{O}_{S_1}^\ell &= (\bar{q}_L b_R)(\bar{\ell}_R \nu_{\ell L}), \\
\mathcal{O}_{S_2}^\ell &= (\bar{q}_R b_L)(\bar{\ell}_R \nu_{\ell L}), \\
\mathcal{O}_T^\ell &= (\bar{q}_R \sigma^{\mu\nu} b_L)(\bar{\ell}_R \sigma_{\mu\nu} \nu_{\ell L}),
\end{aligned} \tag{3.18}$$

where $q = u$ or c . If we match the ones in Eq. (3.17) with those mentioned in Eq. (2.1) for $b \rightarrow c\ell\nu_\ell$ transition, we find the following relations⁴ among the couplings [44],

$$\frac{C_{lq}^{(3)32}}{\Lambda^2} = -\frac{V_{cb}}{V_{cs}} \left(\frac{C_{V_1}^\ell}{v^2} \right), \quad \frac{C_{lequ}^{(1)32}}{\Lambda^2} = -2 \frac{V_{cb}}{V_{tb}} \left(\frac{C_{S_2}^\ell}{v^2} \right), \quad \frac{C_{lequ}^{(3)32}}{\Lambda^2} = -2 \frac{V_{cb}}{V_{tb}} \left(\frac{C_T^\ell}{v^2} \right). \tag{3.19}$$

FCCC processes like $b \rightarrow q\ell\nu$ have been widely studied on [81, 83–85]. In this analysis, we borrow the constraints from [81], where the experimental results of $\bar{B} \rightarrow D(D^*)\ell^-\bar{\nu}_\ell$, $R(D^{(*)}), \bar{B} \rightarrow \pi\ell^-\bar{\nu}_\ell$ ($\ell = \mu, e$) along with lattice inputs are taken into account. We find that from $b \rightarrow c\mu\nu_\mu$ and $b \rightarrow u\mu\nu_\mu$ decays, the constraints on $\mathcal{O}_{lequ}^{(1)}$ are $C_{lequ}^{(1)32}/\Lambda^2 = (0.09 \pm 0.58) \times 10^{-7} \text{ GeV}^{-2}$ and $C_{lequ}^{(1)31}/\Lambda^2 = (0.02 \pm 0.12) \times 10^{-7} \text{ GeV}^{-2}$ respectively. As the uncertainties are very high here, we may infer that the corresponding operator is insensitive to these decays and zero consistent. $\mathcal{O}_{lequ}^{(3)}$ is also insensitive for these two decay modes for the same reason.

- $P \rightarrow \ell\nu_\ell$ decay: Leptonic decays from pseudoscalar mesons (P) provide one of cleanest probes to constrain NP. The hadronic matrix elements for these decays with different Lorentz structures are defined as [86],

$$\langle 0 | \bar{q}_1 \gamma^\mu \gamma^5 q_2 | P(p) \rangle = i f_P p^\mu, \quad \langle 0 | \bar{q}_1 \gamma^5 q_2 | P(p) \rangle = -i f_P \frac{M_P}{m_{q_1} + m_{q_2}}, \tag{3.20}$$

where m_P , f_P , and $m_{q_{1(2)}}$ are the mass, decay constant, and mass of constituent quarks of P -meson, respectively. These inputs for different pseudoscalar mesons are taken from the FLAG review [71]. $\mathcal{O}_{lq}^{(3)}$ and $\mathcal{O}_{lequ}^{(1)}$ operators contribute to these decays. Using the effective Hamiltonian in Eq. (3.17), the branching ratio of $P \rightarrow \ell\nu_\ell$ is expressed as;

$$\mathcal{B}(P \rightarrow \ell\nu_\ell) = \tau_P \frac{m_P m_\ell f_P^2 G_F^2 V_{q_1 q_2}}{8\pi} \left(1 - \frac{m_\ell^2}{m_P^2} \right)^2 \left| 1 - C_{V_1} + \frac{m_P^2}{m_\ell(m_{q_1} + m_{q_2})} C_{S_2} \right|^2, \tag{3.21}$$

where, τ_P is the lifetime of P meson, m_ℓ is the mass of the lepton (ℓ), and $V_{q_1 q_2}$ is CKM matrix element. C_{V_1} and C_{S_2} follow same relations as expressed in Eq. (3.19). Constraints on C_{V_1} and C_{S_2} couplings are tabulated in Table 3. Using these observables, we note the constraints on C_i/Λ^2 in Table 1 and 2 following Eq. (3.19).

⁴For $b \rightarrow u\ell\nu_\ell$ transition, c index in the CKM matrix elements is replaced by u and the WCs will have ‘31’ flavor indices.

- $t \rightarrow b\ell\nu_\ell$ decay: Along with the flavor observable described above, semi leptonic decays of top quark is instrumental in constraining NP. The $t \rightarrow b\ell\nu_\ell$ decay gets contribution from few operators in Eq. (2.1), thereby imposing constraints on the associated dimension six effective couplings. This decay process is governed by W mediated charge current interaction within SM whereas for NP contribution arises from $\mathcal{O}_{lq}^{(3)}$, $\mathcal{O}_{lequ}^{(1)}$ and $\mathcal{O}_{lequ}^{(3)}$ operators. The total decay width (Γ^t) for this process is given by,

$$\Gamma^t = \frac{1}{64\pi^3 m_t} \int_{E_\ell=0}^{\frac{m_t}{2}} \left(\int_{E_b=(\frac{m_t}{2}-E_\ell)}^{\frac{m_t}{2}} |\mathcal{M}_{\text{tot}}^t|^2 dE_b \right) dE_\ell, \quad (3.22)$$

where m_t is mass of top quark, E_b and E_ℓ are the energy of b-quark and lepton (ℓ), respectively. SM and NP contribution to the total amplitude are written in the appendix. Constraints on $\mathcal{O}_{lq}^{(3)}$ from this decay is tabulated in Table 1. For scalar ($C_{lequ}^{(3)}/\Lambda^2$) and tensor ($C_{lequ}^{(3)}/\Lambda^2$) mediated couplings, orders of the constraints are 10^{-3} and 10^{-4} respectively. For $t \rightarrow c\ell\ell$ decay (Eq. (3.23)), upper limit of these operators is 10^{-5} . Therefore constraints obtained from $t \rightarrow b\ell\nu$ on $C_{lequ}^{(1)}/\Lambda^2$ and $C_{lequ}^{(3)}/\Lambda^2$ are ruled out from $t \rightarrow c\ell\ell$ decay.

As our interest lies mostly in $3 \rightarrow 2$ transitions, WCs of the contributing operators are more constrained from present data involving electron or muon final states compared to tau. However, both electron and muon final states provide similar bounds. Therefore, we do not consider lepton generation indices in the WCs and add indices pertaining to quark sectors only. Utilizing experimental data from various flavor observables and top quark measurements, individual constraints on different WCs are presented in column three of Table 1 and 2. Simultaneous fit is performed to constrain the WCs, incorporating all available flavor violating observables pertaining to specific $i \rightarrow j$ transitions, see column four of Table 1 and 2. If we further perform a simultaneous fit by considering all the flavor violating contributions, then the constraints on vector, scalar, and tensor couplings turn out to be:

$$\begin{aligned} C_{lq}^{(1)32}/\Lambda^2 &= -9.96 \times 10^{-10} \text{ GeV}^{-2}, \\ C_{lequ}^{(1)32}/\Lambda^2 &= -9.27 \times 10^{-10} \text{ GeV}^{-2}, \\ C_{lequ}^{(3)32}/\Lambda^2 &= 7.24 \times 10^{-11} \text{ GeV}^{-2}. \end{aligned}$$

These bounds are of similar order for vector and scalar couplings but more stringent for the tensor one, all of which we probe at the muon collider (Section 4). We would like to note however, that the scalar coupling from $3 \rightarrow 2$ transition are less constrained, $C_{lequ}^{(1)32}/\Lambda^2 \sim 10^{-7} \text{ GeV}^{-2}$, see in Table 2. Therefore, it can be individually probed with less CM energy (preferably at e^+e^- colliders) which we discuss in Section 6. However, with more data for $3 \rightarrow 2$ transition in future, $C_{lequ}^{(1)32}/\Lambda^2$ constraints could reach above mentioned simultaneous fit bound. Note that no suitable observable has been found to constrain \mathcal{O}_{lu} and \mathcal{O}_{eu} operators, resulting an upper bound on them from $t \rightarrow c\ell\ell$ decay, as pointed out in Table 1. We make predictions for $t \rightarrow c\ell\ell$ transition and other flavor observables as we discuss next.

3.2 Prediction on different observables

Using the constraints on the EFT operators obtained in Table 1, Table 2 and Table 3, we provide future prediction of following observables, with numerical estimates noted in Table 4.

- $\mathcal{B}(t \rightarrow c\ell\ell)$: The branching ratio of $t \rightarrow c\ell\ell$ decay is given by⁵,

$$\mathcal{B}(t \rightarrow c\ell\ell) = \frac{m_t^5}{6144\pi^3\Lambda^4\Gamma_{\text{tot}}^t} \left(4(C_{lq}^{(1)32} + C_{lq}^{(3)32})^2 + (C_{eu}^{322} + C_{lu}^{322} + C_{qe}^{322} + C_{lequ}^{(1)322} + 72C_{lequ}^{(3)322}) \right). \quad (3.23)$$

As of now, there hasn't been any specific experimental searches conducted to observe $t \rightarrow c\ell\ell$ decays. However, an indirect upper limit on $t \rightarrow c\ell\ell$ decays can be obtained by $t \rightarrow Zq$ searches at ATLAS [87]. At 95% C.L., bounds on $t \rightarrow c\ell\ell$ branching ratios are [19],

$$\begin{aligned} \mathcal{B}(t \rightarrow ce^+e^-) &< 2.1 \times 10^{-4}, \\ \mathcal{B}(t \rightarrow c\mu^+\mu^-) &< 1.5 \times 10^{-4}. \end{aligned} \quad (3.24)$$

These upper limits of the branching ratio provide upper bounds on the dimension-six effective vector and scalar operators on the order of 10^{-5} whereas for tensor operator the upper bound is 10^{-7} . Constraints determined from experimental inputs on dimension-six effective couplings listed in Table 1 and 2 respect this upper bound. Using the obtained constraints on dimension-six effective couplings, we provide the prediction on this observable in Table 4.

- $\mathcal{B}(K_L \rightarrow \pi^0\ell\bar{\ell})$: The branching fraction of $K_L \rightarrow \pi^0\ell\bar{\ell}$ can be expressed as [88, 89],

$$\mathcal{B}(K_L \rightarrow \pi^0\ell\bar{\ell}) = \left(C_{\text{dir}}^\ell \pm C_{\text{int}}^\ell |a_S| + C_{\text{mix}}^\ell |a_S|^2 + C_{\gamma\gamma}^\ell \right) \cdot 10^{-12}, \quad (3.25)$$

The details of a_S , C_{dir}^ℓ , C_{int}^ℓ , C_{mix}^ℓ and $C_{\gamma\gamma}^\ell$ are discussed in [88, 89]. Constraint on $C_{lq}^{(1)}/\Lambda^2$ and $C_{lq}^{(3)}/\Lambda^2$ couplings provide prediction on this observable.

- $\mathcal{B}(D^0 \rightarrow \mu\mu)$: Branching ratio of $D^0 \rightarrow \mu\mu$ decay is noted as [90],

$$\text{BR}(D^0 \rightarrow \mu\mu) = \frac{M_D}{8\pi\Gamma_D\Lambda^4} \sqrt{1 - \frac{4m_\mu^2}{M_D^2}} \left[\left(1 - \frac{4m_\mu^2}{M_D^2} \right) |A|^2 + |B|^2 \right], \quad (3.26)$$

with,

$$\begin{aligned} A &= \frac{G_F f_D M_D^2}{2m_c} C_{lequ}^{(1)31}, \\ B &= \frac{G_F f_D m_\mu}{2m_c} (C_{lq}^{(1)31} + C_{lq}^{(3)31} - C_{lu}^{31} + C_{qe}^{31}), \end{aligned} \quad (3.27)$$

⁵The expression of $\text{Br}(t \rightarrow c\ell\ell)$ is calculated in the limit of $m_c, m_\ell \rightarrow 0$, but in numerical evaluation all masses are taken into account.

where m_c is the mass of charm quark, M_D and f_D are the mass and decay constant of D^0 , respectively. Tensor mediated operator does not contribute to this observable as $\langle \ell^+ \ell^- | \mathcal{O}_{lequ}^{(3)} | D^0 \rangle = 0$. Constraints on operators written in Eq. (3.27) provide prediction on this observable.

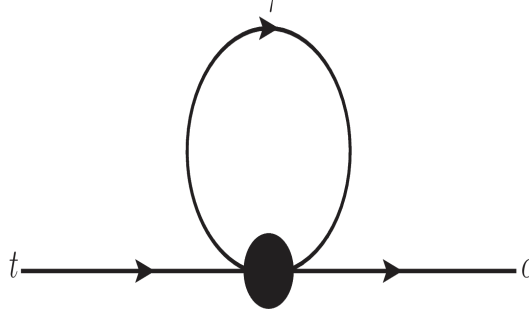


Figure 3: τ mediated 1-loop scalar mediated operator $\mathcal{O}_{lequ}^{(1)}$ contribution to $t \rightarrow c\gamma$ decay where a photon is radiated from t , c leg, and τ loop.

- $\mathcal{B}(t \rightarrow c\gamma)$: Scalar mediated dimension-six effective coupling provides a prediction on $\text{BR}(t \rightarrow c\gamma)$ through τ mediated 1-loop diagram as shown in figure 3. Vector and tensor mediated operators do not contribute to this observable as $\langle c\gamma | \text{any vector operator} | t \rangle = 0$ and $\langle c\gamma | \mathcal{O}_{lequ}^{(3)} | t \rangle = 0$. The expression of $\mathcal{B}(t \rightarrow c\gamma)$ is given by,

$$\mathcal{B}(t \rightarrow c\gamma) = \frac{8e_0^2 m_\tau^6}{9\Gamma^t(m_t^2 - m_c^2)} \left(\frac{C_{lequ}^{(1)32}}{\Lambda^2} \right)^2 \left(1 + 2\text{Log} \left[\frac{\Lambda}{m_\tau} \right] \right)^2 (m_c^4 + 7m_c^2 m_t^2 + m_t^4). \quad (3.28)$$

Prediction on different observables as noted in Table 4 suggests that all the experimental predictions on dimension-six effective couplings are consistent with existing upper bounds.

NP couplings	Related processes/ Observables	Constraints (GeV ⁻²)	Simultaneous fit (GeV ⁻²)
$C_{lq}^{(1)32}/\Lambda^2$	$b \rightarrow s\mu\mu$ $\Delta m_{B_s^0}$ $\mathcal{B}(B_s^0 \rightarrow \mu^+\mu^-)$	$-(3.98 \pm 1.20) \times 10^{-10}$ $-(3.08 \pm 0.01) \times 10^{-8}$ $-(7.39^{+0.41}_{-0.44}) \times 10^{-10}$	$-(4.94 \pm 0.03) \times 10^{-9}$
$C_{lq}^{(1)31}/\Lambda^2$	$b \rightarrow d\mu\mu$ $\Delta m_{B_d^0}$	$-(1.90^{+0.65}_{-0.68}) \times 10^{-10}$ [63] $-(1.81 \pm 0.05) \times 10^{-8}$	$-(5.01 \pm 0.66) \times 10^{-10}$
$C_{lq}^{(1)21}/\Lambda^2$	$\mathcal{B}(K_L \rightarrow \mu^+\mu^-)$ $\mathcal{B}(K^+ \rightarrow \pi^+\nu\bar{\nu})$	$-(1.21^{+0.33}_{-0.31}) \times 10^{-10}$ $-(3.50^{+0.55}_{-0.80}) \times 10^{-10}$	$-(1.21 \pm 0.32) \times 10^{-10}$
$C_{lq}^{(3)32}/\Lambda^2$	$B \rightarrow D^{(*)}\tau\nu_\tau$ $B \rightarrow D^{(*)}\mu(e)\nu$ $b \rightarrow s\mu\mu$ $\mathcal{B}(B_s^0 \rightarrow \mu^+\mu^-)$ $\Delta m_{B_s^0}$	$-(0.35 \pm 0.15) \times 10^{-7}$ [81] $(0.14 \pm 0.09) \times 10^{-7}$ [81] $-(3.98 \pm 1.20) \times 10^{-10}$ $-(7.39^{+0.41}_{-0.44}) \times 10^{-10}$ $-(1.10 \pm 0.01) \times 10^{-8}$	$-(2.15 \pm 0.04) \times 10^{-9}$
$C_{lq}^{(3)31}/\Lambda^2$	$B \rightarrow \pi\mu\nu_\mu$ $b \rightarrow d\mu\mu$ $\mathcal{B}(B^\pm \rightarrow \tau\nu_\tau)$ $\Delta m_{B_d^0}$	$(0.06 \pm 0.20) \times 10^{-7}$ [81] $-(1.90^{+0.65}_{-0.68}) \times 10^{-10}$ [63] $(1.27 \pm 0.43) \times 10^{-7}$ $-(1.81 \pm 0.05) \times 10^{-8}$	$-(5.01 \pm 0.66) \times 10^{-10}$
$C_{lq}^{(3)21}/\Lambda^2$	$\mathcal{B}(K_L \rightarrow \mu^+\mu^-)$ $\mathcal{B}(K^+ \rightarrow \pi^+\nu\bar{\nu})$ $\mathcal{B}(K^\pm \rightarrow \mu\nu_\mu)$ $\mathcal{B}(D^\pm \rightarrow \mu\nu_\mu)$	$-(1.21^{+0.33}_{-0.31}) \times 10^{-10}$ $(3.50^{+0.55}_{-0.80}) \times 10^{-10}$ $(2.21 \pm 0.74) \times 10^{-8}$ $-(1.14 \pm 1.52) \times 10^{-8}$	$(1.63 \pm 0.29) \times 10^{-10}$
$C_{lq}^{(3)11}/\Lambda^2$	$\mathcal{B}(\pi^\pm \rightarrow \mu\nu_\mu)$	$(1.28 \pm 0.81) \times 10^{-8}$	
$C_{lq}^{(3)22}/\Lambda^2$	$\mathcal{B}(D_s^\pm \rightarrow \mu\nu_\mu)$	$(6.02 \pm 9.94) \times 10^{-9}$	
$C_{lq}^{(3)33}/\Lambda^2$	$\mathcal{B}(t \rightarrow b\ell\nu_\ell)$	$(7.13 \pm 0.37) \times 10^{-7}$	
C_{eu}^{32}/Λ^2	$t \rightarrow c\ell\ell$	$< 10^{-5}$ [19]	-
C_{lu}^{32}/Λ^2	$t \rightarrow c\ell\ell$	$< 10^{-5}$ [19]	-
C_{qe}^{32}/Λ^2	$b \rightarrow s\mu\mu$ $\mathcal{B}(B_s^0 \rightarrow \mu^+\mu^-)$ $\Delta m_{B_s^0}$	$-(1.24 \pm 0.26) \times 10^{-9}$ $-(7.39^{+0.415}_{-0.445}) \times 10^{-10}$ $-(1.10 \pm 0.01) \times 10^{-8}$	$-(1.01 \pm 0.02) \times 10^{-9}$
C_{qe}^{31}/Λ^2	$b \rightarrow d\mu\mu$ $\Delta m_{B_d^0}$	$(0.68^{+2.72}_{-2.79}) \times 10^{-10}$ [63] $-(1.81 \pm 0.05) \times 10^{-8}$	$-(4.15 \pm 0.24) \times 10^{-9}$
C_{qe}^{21}/Λ^2	$\mathcal{B}(K_L \rightarrow \mu^+\mu^-)$	$-(1.213^{+0.334}_{-0.310}) \times 10^{-10}$	

Table 1: Constraints on the different dimension-six effective vector couplings from various flavor and top-quark processes and decay modes. For the details on observables concerning $b \rightarrow s\mu^+\mu^-$ and $b \rightarrow d\mu^+\mu^-$ transitions, see references [49, 63] and for the measurements see the text.

NP couplings	Related processes/ Observables	Constraints (GeV ⁻²)	Simultaneous fit (GeV ⁻²)
$C_{lequ}^{(1)32}/\Lambda^2$	$B \rightarrow D^{(*)}\tau\nu_\tau$	$(1.81 \pm 0.06) \times 10^{-7}$ [81]	$(1.79 \pm 0.06) \times 10^{-7}$
	$B \rightarrow D^{(*)}\mu\nu_\mu$	$(0.09 \pm 0.58) \times 10^{-7}$ [81]	
	$B \rightarrow D^{(*)}e\nu_e$		
$C_{lequ}^{(1)31}/\Lambda^2$	$B \rightarrow \pi\mu\nu_\mu$ $B \rightarrow \pi e\nu_e$	$(0.03 \pm 0.18) \times 10^{-7}$ [81]	$-(6.64 \pm 0.21) \times 10^{-9}$
	$\mathcal{B}(B^\pm \rightarrow \tau\nu_\tau)$	$-(6.64 \pm 0.21) \times 10^{-9}$	
$C_{lequ}^{(1)21}/\Lambda^2$	$\mathcal{B}(D^\pm \rightarrow \mu\nu_\mu)$ $\mathcal{B}(K^\pm \rightarrow \mu\nu_\mu)$	$-(8.61 \pm 0.18) \times 10^{-10}$ $-(1.83 \pm 0.05) \times 10^{-9}$	$-(9.72 \pm 0.17) \times 10^{-10}$
$C_{lequ}^{(1)11}/\Lambda^2$	$\mathcal{B}(\pi^\pm \rightarrow \mu\nu_\mu)$	$-(5.82 \pm 0.31) \times 10^{-10}$	
$C_{lequ}^{(1)22}/\Lambda^2$	$\mathcal{B}(D_s^\pm \rightarrow \mu\nu_\mu)$	$-(4.36 \pm 3.17) \times 10^{-10}$	
$C_{lequ}^{(3)32}/\Lambda^2$	$B \rightarrow D^{(*)}\tau\nu_\tau$	$(0.62 \pm 0.17) \times 10^{-7}$ [81]	$(0.61 \pm 6.60) \times 10^{-10}$
	$B \rightarrow D^{(*)}\mu\nu_\mu$	$-(0.33 \pm 6.61) \times 10^{-10}$ [81]	
	$B \rightarrow D^{(*)}e\nu_e$		
$C_{lequ}^{(3)31}/\Lambda^2$	$B \rightarrow \pi\mu\nu_\mu$ $B \rightarrow \pi e\nu_e$	$(0.07 \pm 0.16) \times 10^{-7}$ [81]	

Table 2: Constraints of scalar and tensor mediated dimension-six effective couplings from various flavor observables, see text for details.

Decay modes	Branching ratio	Constraints (GeV ⁻²)	
		C_{V_1}	C_{S_2}
$\pi^\pm \rightarrow \mu\nu_\mu$	$(99.9877 \pm 0.00004) \times 10^{-2}$	$-(1.77 \pm 0.6) \times 10^{-2}$	$(4.33 \pm 0.23) \times 10^{-4}$
$K^\pm \rightarrow \mu\nu_\mu$	$(63.56 \pm 0.11) \times 10^{-2}$	$-(3.21 \pm 1.08) \times 10^{-2}$	$(1.36 \pm 0.04) \times 10^{-3}$
$B^\pm \rightarrow \tau\nu_\tau$	$(1.09 \pm 0.24) \times 10^{-4}$	$-(1.85 \pm 0.62) \times 10^{-1}$	$(4.94 \pm 1.60) \times 10^{-2}$
$D_s^\pm \rightarrow \mu\nu_\mu$	$(5.43 \pm 0.15) \times 10^{-3}$	$-(8.74 \pm 14.43) \times 10^{-3}$	$(3.25 \pm 2.36) \times 10^{-4}$
$D^\pm \rightarrow \mu\nu_\mu$	$(3.74 \pm 0.17) \times 10^{-4}$	$(1.66 \pm 2.21) \times 10^{-2}$	$-(6.40 \pm 8.71) \times 10^{-4}$

Table 3: Constraints on C_{V_1} and C_{S_2} from $\mathcal{B}(P \rightarrow \ell\nu_\ell)$. Experimental inputs for different $P \rightarrow \ell\nu_\ell$ branching ratios are adopted from the PDG average [80].

Dimension-six couplings	Observables	Branching ratio	
		Prediction	Upper bound
$C_{lq}^{(1)32}/\Lambda^2$	$\mathcal{B}(K_L \rightarrow \pi^0 e^+ e^-)$	7.38×10^{-11}	2.8×10^{-10} [91]
	$\mathcal{B}(K_L \rightarrow \pi^0 \mu^+ \mu^-)$	8.43×10^{-11}	3.8×10^{-10} [92]
	$\mathcal{B}(D^0 \rightarrow \mu\mu)$	4.63×10^{-23}	3.1×10^{-9} [93]
	$\mathcal{B}(t \rightarrow cee)$	1.28×10^{-11}	2.1×10^{-4} [19]
	$\mathcal{B}(t \rightarrow c\mu\mu)$	1.30×10^{-11}	1.5×10^{-4} [19]
$C_{lq}^{(3)32}/\Lambda^2$	$\mathcal{B}(K_L \rightarrow \pi^0 e^+ e^-)$	7.42×10^{-11}	2.8×10^{-10} [91]
	$\mathcal{B}(K_L \rightarrow \pi^0 \mu^+ \mu^-)$	8.46×10^{-11}	3.8×10^{-10} [92]
	$\mathcal{B}(D^0 \rightarrow \mu\mu)$	4.63×10^{-21}	3.1×10^{-9} [93]
	$\mathcal{B}(t \rightarrow cee)$	1.31×10^{-11}	2.1×10^{-4} [19]
	$\mathcal{B}(t \rightarrow c\mu\mu)$	1.33×10^{-11}	1.5×10^{-4} [19]
C_{qe}^{32}/Λ^2	$\mathcal{B}(D^0 \rightarrow \mu\mu)$	4.04×10^{-21}	3.1×10^{-9} [93]
	$\mathcal{B}(t \rightarrow cee)$	2.79×10^{-12}	2.1×10^{-4} [19]
	$\mathcal{B}(t \rightarrow c\mu\mu)$	2.82×10^{-12}	1.5×10^{-4} [19]
$C_{lequ}^{(1)32}/\Lambda^2$	$\mathcal{B}(t \rightarrow cee)$	4.60×10^{-13}	2.1×10^{-4} [19]
	$\mathcal{B}(t \rightarrow c\mu\mu)$	4.66×10^{-13}	1.5×10^{-4} [19]
	$\mathcal{B}(t \rightarrow c\gamma)$	8.45×10^{-17}	1.8×10^{-4} [94]
$C_{lequ}^{(3)32}/\Lambda^2$	$\mathcal{B}(t \rightarrow cee)$	2.84×10^{-13}	2.1×10^{-4} [19]
	$\mathcal{B}(t \rightarrow c\mu\mu)$	2.86×10^{-13}	1.5×10^{-4} [19]

Table 4: Prediction of different observables using more conservative flavor constraints WCs from the simultaneous fit using all possible the flavor violating contributions and existing upper bound.

4 Collider analysis

In this section, we analyze the possibility of probing the NP at collider in terms of the effective operators as in Eq. (2.1). For that we focus on those most stringent limits of the dimension-six effective operators stemmed from the flavor observables. If the most stringent limits on the NP couplings can be probed for a given \sqrt{s} then the others can be probed at a smaller \sqrt{s} . From Section 3.1, we see that the flavor constraint on $C_{lequ}^{(3)32}/\Lambda^2$, the tensor coupling is one of the most stringent ones which are on the order of $\sim 10^{-11} \text{ GeV}^{-2}$ followed by a conservative estimate of $C_{lequ}^{(1)32}/\Lambda^2 \sim 10^{-9} \text{ GeV}^{-2}$ and $C_{lq}^{(1)32}/\Lambda^2 \sim 10^{-9} \text{ GeV}^{-2}$. Therefore, in our subsequent analysis, we will focus on these three WCs mostly. From Eq. (4.2), it is clear that the signal cross-section exhibits a linear growth with the square of the CM energy, conversely, SM background processes are expected to decrease as \sqrt{s} increases. Therefore, at high \sqrt{s} , a muon collider should have the capability to detect a such NP scenarios where the CM energy of the machine is expected to go upto 30 TeV. For our analysis, we consider $\sqrt{s} = 10 \text{ TeV}$ with an integrated luminosity ($\mathfrak{L}_{\text{int}}$) of 1 ab^{-1} . This choice is within the reach of the future muon collider projections [20]. We further note that when we are probing $C/\Lambda^2 \sim 10^{-11} \text{ GeV}^{-2}$ at $\sqrt{s} = 10 \text{ TeV}$, we assume, $\Lambda \gtrsim 10 \text{ TeV}$, so that the WC $C \gtrsim 10^{-3}$, to keep the effective theory framework validated. As mentioned before, the constraint on scalar operator $C_{lequ}^{(1)32}/\Lambda^2$ from $3 \rightarrow 2$ transition observable is less stringent, therefore, it can be probed at the electron-positron colliders at much lower CM energy, which we discuss in Section 6.

4.1 $t\bar{c}(\bar{t}c + t\bar{c})$ production cross-section

The differential $t\bar{c}(\bar{t}c)$ production cross-section at $\mu^+\mu^-$ collider, governed by the effective four-Fermi contact interaction as shown in figure 1, in terms of vector, scalar and tensor couplings is given by⁶,

$$\frac{d\sigma}{d\cos\theta} = \frac{3\mathcal{F}}{8} \left\{ 2(\mathcal{V}_{RR}^2 + \mathcal{V}_{LL}^2) \left(1 + (1 + \beta) \cos\theta + \beta \cos^2\theta \right) + 2(\mathcal{V}_{RL}^2 + \mathcal{V}_{LR}^2) \left(1 - (1 + \beta) \cos\theta + \beta \cos^2\theta \right) \right. \\ \left. + \mathcal{S}_{RR}^2(1 + \beta) - 4\mathcal{S}_{RR}\mathcal{T}_{RR}(1 + \beta) \cos\theta + 16\mathcal{T}_{RR}^2(1 - \beta + 2\beta \cos^2\theta) \right\}, \quad (4.1)$$

where $\mathcal{F} = \frac{s}{\Lambda^4} \frac{\beta^2}{4\pi(1+\beta^3)}$ and $\beta = \frac{s-m_t^2}{s+m_t^2}$. Therefore, total production cross-section is,

$$\sigma_{\text{prod}} = \mathcal{F} \left[8\mathcal{T}_{RR}^2(3 - \beta) + \frac{3}{2}\mathcal{S}_{RR}^2 + (\mathcal{V}_{LL}^2 + \mathcal{V}_{RR}^2 + \mathcal{V}_{LR}^2 + \mathcal{V}_{RL}^2)(3 + \beta) \right]. \quad (4.2)$$

The variation of the signal cross-section (σ_{prod}) for the vector, scalar and tensor four Fermi operators used in this model with CM energy (\sqrt{s}) is shown in the right side of the figure 4. Here, $\Lambda = 50 \text{ TeV}$ and WCs ($C = 1$) are kept constants. From Eq. (4.1) we see that the total cross-section (σ_{prod}) is proportional to s/Λ^4 , therefore, larger CM energy yields larger cross-section, provided we are in the effective theory limit, i.e. $\sqrt{s} < \Lambda$. We also note from figure 4, that the production cross-section is largest for the tensor coupling and the lowest

⁶In the expression of differential cross-section, muon mass is neglected.

for the vector coupling. For vector coupling, the cross-section ~ 0.1 fb at $\sqrt{s} = 5$ TeV and that is down to 0.001 fb at $\sqrt{s} = 1$ TeV for $C/\Lambda^2 \sim 10^{-10}$ GeV $^{-2}$, making it a necessity to probe these couplings at $\sqrt{s} = 10$ TeV. The variation is shown in one operator scenario, that implies $\sigma_{\text{prod}} \propto C_i^2/\Lambda^4$. Therefore the variation of total cross-section with C/Λ^2 is symmetric as depicted in the left side of figure 1. Apart from the four-Fermi couplings, Ztc couplings (a_L^Z and a_R^Z) via $\mathcal{O}_{\phi q}^{(1)}$, $\mathcal{O}_{\phi q}^{(3)}$ and $\mathcal{O}_{\phi u}$ also contribute to tc production by interfering with the four-Fermi vector couplings \mathcal{V}_{ij} . The contribution of Ztc couplings can be incorporated to the total cross-section by redefining,

$$\mathcal{V}_{ij} \rightarrow \mathcal{V}_{ij} + 4c_i^Z a_j^Z \frac{m_W m_Z}{s - m_Z^2} \quad \text{with} \quad a_L^Z = \frac{1}{4c_w}(C_{\phi q}^{(1)} - C_{\phi q}^{(3)}), \quad a_R^Z = \frac{1}{4c_w}C_{\phi u}, \quad (4.3)$$

where, $i, j = L, R$, and $c_L^Z = -1/2 + s_w^2$ and $c_R^Z = s_w^2$ are the couplings to a left or right

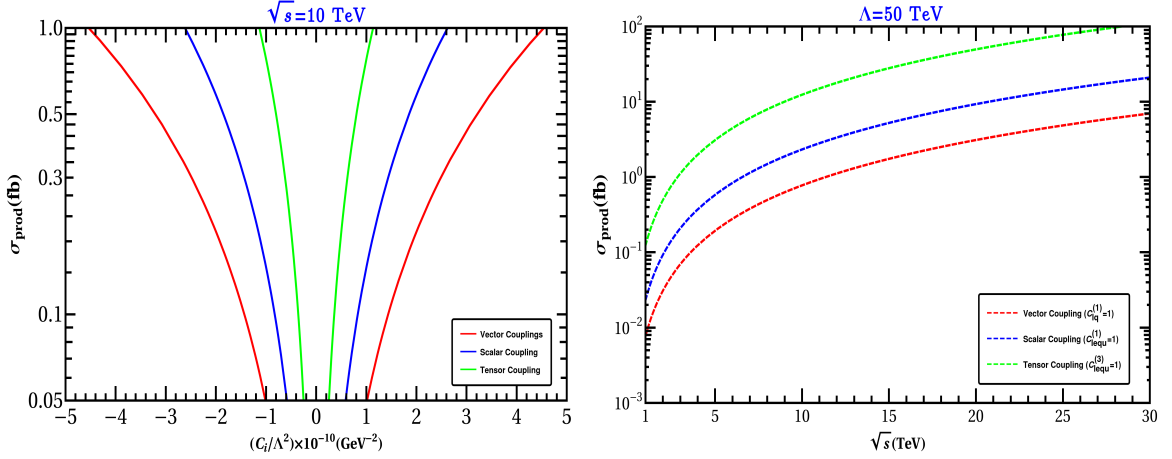


Figure 4: Variation of total cross-section of tc production at $\mu^+\mu^-$ collider with different choices of C/Λ^2 (GeV $^{-2}$) (left) and CM energy (\sqrt{s}) for $\Lambda = 50$ TeV (right).

handed electron, respectively. On contrary to four-Fermi couplings, the cross-section via Z mediation drops as $\sim 1/s$ due to the s-channel mediation. In the left side of figure 4, we show the variation of σ_{prod} with varying C/Λ^2 in GeV $^{-2}$. From the figure, we again see that the tensor mediated four-Fermi coupling (\mathcal{T}_{RR}) provides the maximum contribution to the tc production and vector mediated production provides the least. In one operator scenario, all the vector operator contribute equally to the total cross-section. If we assume Ztc effective couplings to be of the same order to that of vector coupling, $C/\Lambda^2 \sim 10^{-9}$ GeV $^{-2}$, then the contribution from Ztc is way milder than the four-Fermi operator contribution, see Table 5, where we see that the production cross-section (σ_{prod}) for vector coupling surpasses that of Ztc coupling by an order of 10^8 in fb at 10 TeV muon collider. Therefore in the following analysis we neglect the contribution of Ztc and study the four-Fermi operators. We refrain from studying dimension-eight contributions, which in principle could contribute at the same order as our considered dimension-six contributions.

Couplings (GeV^{-2})	Cross-section (σ_{prod}) (fb)
$C_{lq}^{(1)32}/\Lambda^2$	4.8×10^{-2}
$C_{lequ}^{(1)32}/\Lambda^2$	0.15
$C_{lequ}^{(3)32}/\Lambda^2$	0.77
$C_{\phi q}^{(1)32}/\Lambda^2$	1.71×10^{-10}

Table 5: $t\bar{c}(t\bar{c})$ production cross-section (σ_{prod}) at muon collider for vector ($C_{lq}^{(1)32}/\Lambda^2$), scalar ($C_{lequ}^{(1)32}/\Lambda^2$), tensor ($C_{lequ}^{(3)32}/\Lambda^2$), and Ztc ($C_{\phi q}^{(1)32}/\Lambda^2$) effective couplings. We consider $\sqrt{s} = 10$ TeV and $C/\Lambda^2 = 10^{-10} \text{ GeV}^{-2}$ for all the operators.

4.2 Signal and background processes

In high-energy muon colliders, collision events take place at a CM energy surpassing that achieved by the present LHC (parton level) or potential future electron-positron colliders. Consequently, it is anticipated that jets which are closely clustered together in these collisions, will exhibit collimation, effectively coalescing into a singular, consolidated jet. A notable illustration of this behavior can be observed in the jets stemming from the hadronic decay processes of top quarks or W/Z bosons, where they converge to form a single “top” or “W/Z” jet [95]. Since, the signal process is $\mu^- \mu^+ \rightarrow tc$ (by tc production we always mean $\bar{t}c + t\bar{c}$ production), for this analysis, we consider a di-jet signal with no leptons. The corresponding SM background processes are $\mu^- \mu^+ \rightarrow t\bar{t}$, $\mu^- \mu^+ \rightarrow q\bar{q}$, $\mu^- \mu^+ \rightarrow c\bar{c}$, $\mu^- \mu^+ \rightarrow b\bar{b}$, $\mu^- \mu^+ \rightarrow W^+ W^-$ and $\mu^- \mu^+ \rightarrow ZZ$.

4.2.1 Event simulation

The signal and background events are generated in **MadGraph5** [96]. For the EFT signal process, the UFO model file is generated using **FeynRules** [97]. The benchmark points (BPs) we consider for collider analysis are:

- BP1 (Vector) : $C_{lq}^{(1)32}/\Lambda^2 = -9.96 \times 10^{-10} \text{ GeV}^{-2}$,
- BP2 (Scalar) : $C_{lequ}^{(1)32}/\Lambda^2 = -9.27 \times 10^{-10} \text{ GeV}^{-2}$,
- BP3 (Tensor) : $C_{lequ}^{(3)32}/\Lambda^2 = 7.24 \times 10^{-11} \text{ GeV}^{-2}$.

These BPs are most stringent flavor constrained vector, scalar, and tensor couplings as noted in Table 1 and 2. Using these numerical inputs, Monte-Carlo (MC) generated events are fed into **Pythia8** [98] and **Delphes3** [99] for parton showering and detector simulation, respectively. For event simulation, following criteria are used:

- The lepton selection is done in **Delphes3** with criteria $p_T > 10$ GeV. Further, we impose $|\eta| \leq 2.5$ for electrons and $|\eta| \leq 2.4$ for muons. For electrons, in the allowed $|\eta|$ region, the detection efficiencies are 0.95 in $|\eta| \leq 1.5$ region and 0.85 in $1.5 < |\eta| \leq 2.5$ region. For muon the detection efficiency is 0.95 throughout the allowed region. The lepton isolation criteria is set $\Delta R > 0.5$ from another lepton or jet.

- The jet clustering has been done in `Fastjet3` [100] using `anti-kt` algorithm [101]. The jet radius is taken to be 0.5 with the minimum p_T of the jet set as 20 GeV. The jet reconstruction is done using `Delphes3`.

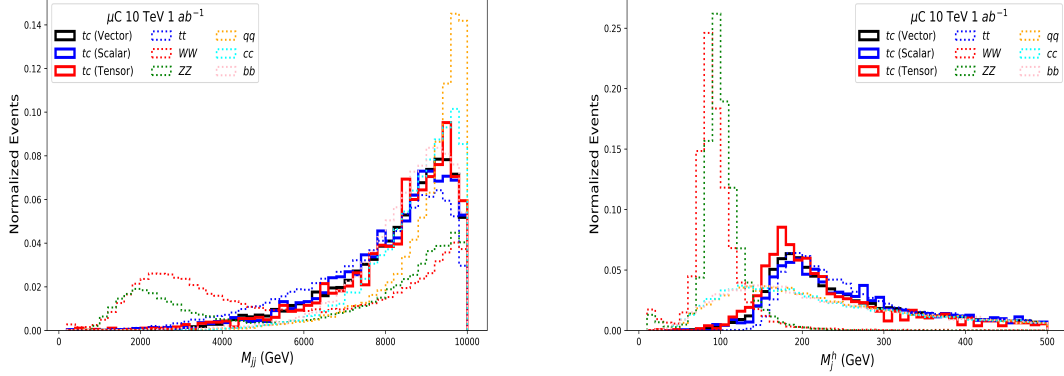


Figure 5: Normalized event distribution for invariant di-jet mass (M_{jj}) (left) and heavy jet mass (M_j^h) (right) in case of di-jet final state containing signal and background processes at the muon collider with $\sqrt{s} = 10 \text{ TeV}$ and $\mathcal{L}_{\text{int}} = 1 \text{ ab}^{-1}$.

4.3 Cut based Analysis

For the analysis, we use the following sequential cuts for the signal and background processes:

- Cut 1: $N_j = 2$ and $N_l = 0$.
- Cut 2: $M_{jj} > 8 \text{ TeV}$.
- Cut 3: $M_j^h > 160 \text{ GeV}$.

Here, M_{jj} is the invariant mass of the di-jet, M_j^h is the invariant masses of the reconstructed particles of the heavier jet. The major background, in case of our analysis, are the diboson processes. In Cut 1, which is our signal selection cut, we demand only processes with 2 jets. We further remove events with detected leptons. This will remove the detected leptonic and semi-leptonic decay processes for W^+W^- , ZZ as well as $t\bar{t}$. The invariant mass of the di-jet pair is expected to peak near the CM energy of the incoming particles for jets coming from the production level processes. For jets coming from branching or radiation, the invariant mass is expected to peak at a lower value. Imposing Cut 2, we can remove further semileptonic and leptonic processes from di-boson production, where the leptons were not detected. Now, due to the collimation of boosted jets in high energies, as we mention above, we expect multiple jets branching from top or W/Z to appear as a single jet in the detector. The invariant mass of the reconstructed particles of such jets are expected to peak at the mass of their respective sources, i.e. top mass or W/Z mass. In tc signal process, the heavier jet is expected to peak at the top mass, as such Cut 3,

will significantly remove W^+W^- and ZZ backgrounds as evident from the distribution in figure 5. The signal can be further separated from the background by using a charm tagging algorithm on the lighter jet of tc signal process. However, with the current c-tagging efficiency at the LHC [102, 103], it looks like a far-fetched possibility. This is primarily due to high miss-tagging efficiency of the b-jets as c-jets. After employing sequential cuts as mentioned above, signal significance $S/\sqrt{S+B}$ and efficiency factor⁷ $\epsilon_{s(b)} = \sigma_{s(b)}^{\text{sig}}/\sigma_{s(b)}^{\text{prod}}$ are noted in Table 6. We see that the benchmark point with vector couplings have most signal significance, while the tensor one has the least.

Process	No Cuts	Cut 1	Cut 2	Cut 3	$\epsilon_{s/b}$	Significance
$\mu^-\mu^+ \rightarrow tc$ (BP1)	6432	1339	891	809	0.12	BP1: 18.40
$\mu^-\mu^+ \rightarrow tc$ (BP2)	4189	918	594	547	0.13	
$\mu^-\mu^+ \rightarrow tc$ (BP3)	140	30	20	18	0.13	
$\mu^-\mu^+ \rightarrow t\bar{t}$	1730	352	191	183	0.10	BP2: 13.38
$\mu^-\mu^+ \rightarrow q\bar{q}$	3555	746	650	433	0.12	
$\mu^-\mu^+ \rightarrow c\bar{c}$	1728	363	290	190	0.11	
$\mu^-\mu^+ \rightarrow b\bar{b}$	914	194	143	93	0.10	BP3: 0.53
$\mu^-\mu^+ \rightarrow W^+W^-$	58860	22882	7258	215	0.004	
$\mu^-\mu^+ \rightarrow ZZ$	3284	1238	454	10	0.003	

Table 6: Cut flow and signal significance for signal at the chosen benchmark points and background processes for analysis at muon collider at 10 TeV and 1 ab^{-1} . Here $\epsilon_{s/b}$ denotes the cut efficiency for signal and background following the final cut (Cut 3).

5 Optimal Observable Technique

The optimal observable technique (OOT) is a statistical tool that enables optimal estimation of NP couplings via minimizing the covariance matrix, which has been used studied for different cases, but mostly without a non-interfering SM background [26–29]. In general, a collider observable (*e.g.*, differential cross-section) contains contribution from both the signal and background. If we wish to write the observable at the production level having the cut efficiencies of signal analysis embedded, then it can be written as,

$$\mathcal{O} = \frac{d\sigma_{\text{theo}}}{d\phi} = \epsilon_s \mathcal{O}_{\text{sig}} + \epsilon_b \mathcal{O}_{\text{bkg}} = \sum_i g_i f_i(\phi). \quad (5.1)$$

Here g_i are the non-linear functions of NP couplings and f_i are the function of phase-space co-ordinate ϕ and ϵ_s (ϵ_b) is the signal (background) efficiencies in estimating the signal (and background) after using judicious cuts as tabulated in Table 6. In this analysis as our focus on $2 \rightarrow 2$ processes, the phase space co-ordinate will be $\phi = \cos\theta$, where θ is angle between the outgoing particles with respect to the beam axis. However, the choice of ϕ can vary depending on the specific process. We importantly note that the

⁷ $\sigma_{s(b)}^{\text{sig}}$ is the final state cross-section after final for signal (background) whereas $\sigma_{s(b)}^{\text{prod}}$ is the production cross-section for signal (background).

signal of the processes under consideration are essentially di-jet events (as elaborated in the previous section), stemming from the produced particles in the high CM energy of the muon collider, enabling us to use Eq. (5.1), without much problem. However, for processes where the decay products are not collimated, say for example, at smaller CM energy, the usage of Eq. (5.1) is limited. For a generic procedure of inclusion of SM background, see [104].

The essential idea is to determine the NP coefficients g_i as precisely as possible. In case of a realistic experimental scenario, the event numbers obey Poisson distribution, we can estimate g_i with the application of appropriate weighting functions ($w_i(\phi)$),

$$g_i = \int w_i(\phi) \mathcal{O}(\phi) d\phi. \quad (5.2)$$

There's one particular choice of $w_i(\phi)$ that optimizes the covariance matrix (\mathbb{V}_{ij}) in a sense that statistical uncertainties in g_i 's are minimal. In this case, \mathbb{V}_{ij} is expressed as:

$$\mathbb{V}_{ij} = \frac{\mathbb{M}_{ij}^{-1} \sigma_T}{N} = \mathbb{M}_{ij}^{-1} \mathfrak{L}_{\text{int}}^{-1}, \quad \mathbb{M}_{ij} = \int \frac{f_i(\phi) f_j(\phi)}{\mathcal{O}(\phi)} d\phi. \quad (5.3)$$

Then, the optimal covariance matrix reads

$$\mathbb{V}_{ij} = \frac{\mathbb{M}_{ij}^{-1} \sigma_T}{N} = \frac{\mathbb{M}_{ij}^{-1}}{\mathfrak{L}_{\text{int}}}, \quad (5.4)$$

with $\sigma_T = \int \mathcal{O}(\phi) d\phi$ defining the total cross-section and N is total number of events ($N = \sigma_T \mathfrak{L}_{\text{int}}$) including the SM background contributions. $\mathfrak{L}_{\text{int}}$ indicates the integrated luminosity of the collider over a period. The χ^2 function, which quantifies the precision of NP couplings, is defined as:

$$\chi^2 = \sum_{\{i,j\}=1}^n (g_i - g_i^0)(g_j - g_j^0) \left(\mathbb{V}^{-1} \right)_{ij}, \quad (5.5)$$

where g^0 's are the ‘seed values’ of NP model inputs. Here we use them as the ones predicted from the flavor constraints.

5.1 OOT Sensitivities

Here, we discuss the optimal uncertainties and correlations of different dimension-six effective operators in context of $t\bar{c}(\bar{t}c)$ production. As mentioned before, we focus on the probe of most stringent vector, scalar, and tensor mediated couplings that contribute to the tc production at the $\mu^+\mu^-$ colliders. The χ^2 variation dimension-six effective operators are shown in the figure 6. At CM energy $\sqrt{s}=10$ TeV and luminosity $\mathfrak{L}_{\text{int}} = 1 \text{ ab}^{-1}$, we observe that for all the couplings, optimal uncertainty is narrower than flavor uncertainty. It is intriguing to note that for the tensor-mediated coupling $C_{lequ}^{(3)32}/\Lambda^2$, the flavor uncertainty is way larger than the optimal collider sensitivity of this coupling at muon collider (see the right most panel in figure 6). This suggests that the pertinent operator is less-consistent in

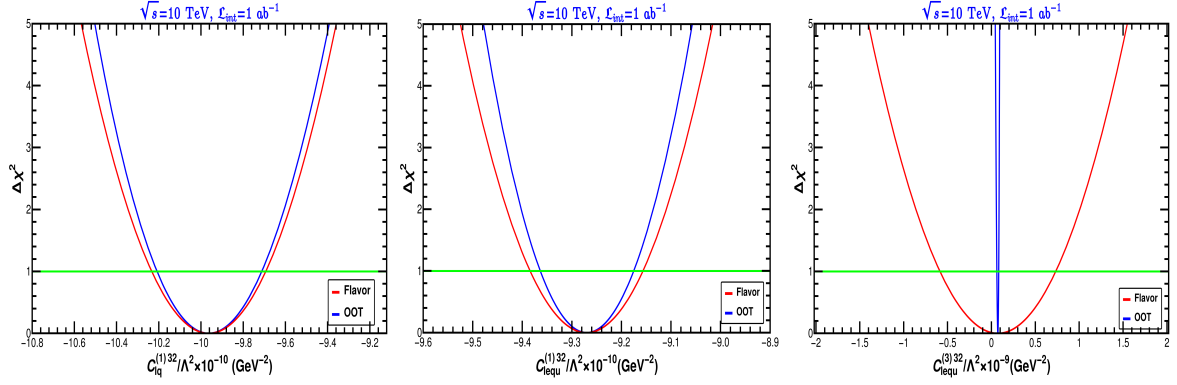


Figure 6: The $\Delta\chi^2$ variation as a function of dimension-six effective couplings; left: $C_{lq}^{(1)32}/\Lambda^2$ (Vector), middle: $C_{lequ}^{(1)32}/\Lambda^2$ (Scalar), right: $C_{lequ}^{(3)32}/\Lambda^2$ (Tensor). The units of C^{ij}/Λ^2 is in GeV^{-2} . The horizontal green axis denotes $\Delta\chi^2 = 1$.

flavor observable, yet in a collider scenario, it can be measured with larger precision. This is because the tensor operator having most stringent flavor bound, has the largest contribution to the tc production compared to scalar and vector operators, as already evidenced by figure 4 and Table 5.

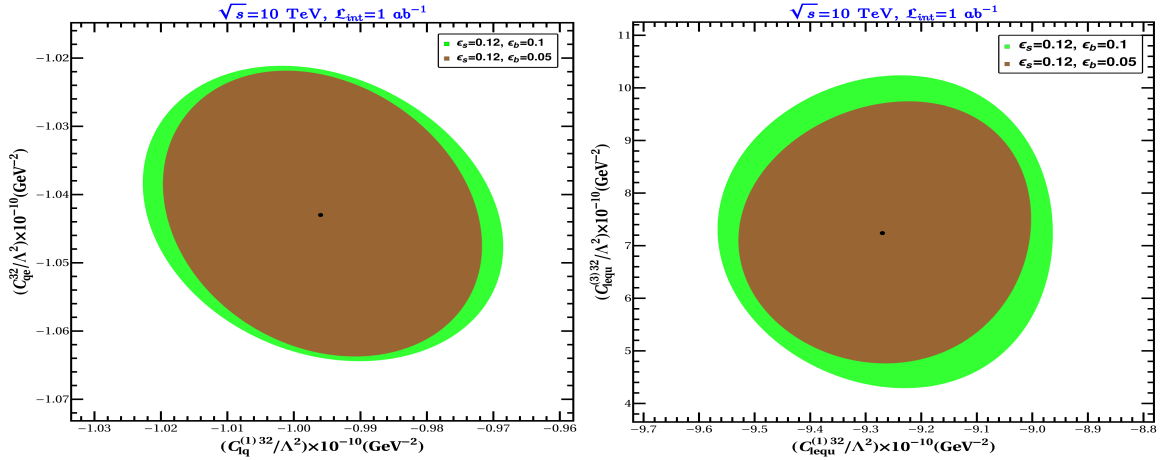


Figure 7: Optimal 1σ allowed parameter space in 2D plane. Left: $C_{lq}^{(1)32}/\Lambda^2 - C_{qe}^{32}/\Lambda^2$ plane; right: $C_{lequ}^{(1)32}/\Lambda^2 - C_{lequ}^{(3)32}/\Lambda^2$ plane. Variation of background efficiency (ϵ_b) is also shown in both cases. See inset and headings for details. The flavor inputs are taken from the case-III mentioned in Table 7.

The correlations between the two vector couplings and correlations among scalar and tensor couplings for different background efficiencies ($\epsilon_b = \{0.1, 0.05\}$) are shown in figure 7. The benchmark cases with seed values are listed in Table 7. It is clear that the presence

of background via ϵ_b plays a crucial role in determining the optimal uncertainty of NP couplings, the lesser the contamination, the better the precision. Moreover, the optimal uncertainty of NP couplings depends on the relative NP signal and non-interfering SM background contribution to the final state. Contribution to the final state from two vectors operators is greater than the scalar and tensor operators together by a factor of 25 (Table 6), due to the choice of the seed values of the benchmark points. Therefore, the relative NP signal is larger than the background contribution for the vector operators than the scalar and tensor ones. That is why the vector operator correlation is less affected by the change in background contamination as shown in the figure 7.

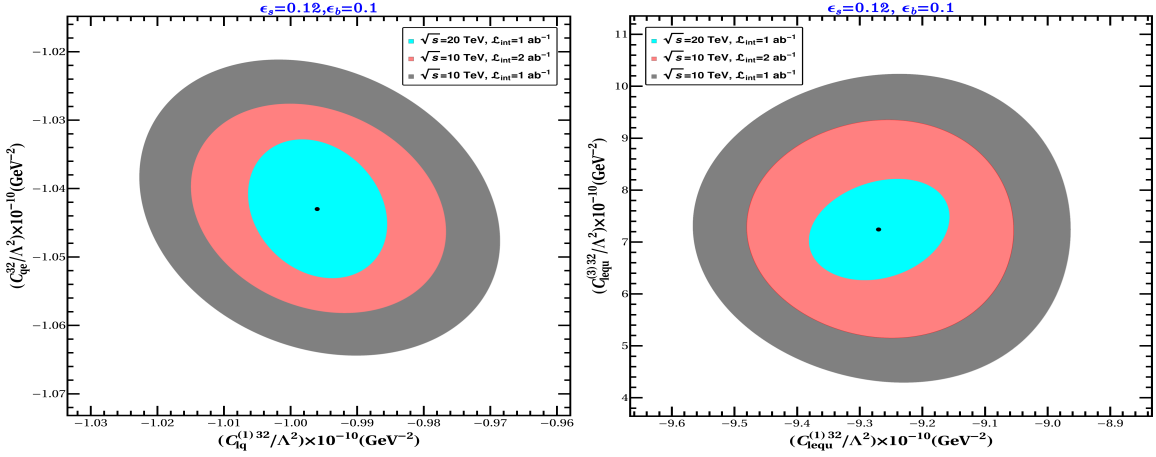


Figure 8: Comparison of optimal 1σ surfaces for CM energy (\sqrt{s}) and luminosity (\mathcal{L}_{int}); Left: $C_{lq}^{(1)32}/\Lambda^2 - C_{qe}^{32}/\Lambda^2$ plane; right: $C_{lequ}^{(1)32}/\Lambda^2 - C_{lequ}^{(3)32}/\Lambda^2$ plane. The flavor inputs are taken from the case-III mentioned in Table 7.

In figure 8 we show the variation of 1σ regions for different CM energies and integrated luminosities. In our scenario, the increase of CM energy (\sqrt{s}) is more effective than the increase of integrated luminosity. If we increase the CM energy twice, then the signal cross-section is increased by a factor of 4 which in turn suggest four times enhancement in signal events. However, we must remember that when we enhance \sqrt{s} , we choose $\Lambda > \sqrt{s}$ to be consistent with EFT framework, reducing the WC appropriately to keep C/Λ^2 is same ballpark. Larger CM energy also reduces the non-interfering SM backgrounds. However, if we double the luminosity, both the signal and background events will enhance twice, suggesting larger CM energy helps reducing optimal uncertainty for EFT frameworks as considered here.

In figure 9, we show the optimal statistical separation of different cases listed in Table 7 from the ‘base model’ SM. Here, Case-I and Case-II are followed from flavor constraints noted in Table 1 and 2 and case-III is considered to show the correlations among different operators. We consider the CM energy $\sqrt{s} = 10$ TeV and integrated luminosity $\mathcal{L}_{\text{int}} = 1$ ab^{-1} . We determine that for various vector (scalar and tensor) operator combinations,

Cases	Vector ops. combination	Scalar and tensor ops. combination
I	$\frac{C_{lq}^{(1)32}}{\Lambda^2} = -9.96 \times 10^{-10} \text{ GeV}^{-2},$ $\frac{C_{qe}^{32}}{\Lambda^2} = 0$	$\frac{C_{lequ}^{(1)32}}{\Lambda^2} = -9.27 \times 10^{-10} \text{ GeV}^{-2},$ $\frac{C_{lequ}^{(3)32}}{\Lambda^2} = 0$
II	$\frac{C_{lq}^{(1)32}}{\Lambda^2} = 0,$ $\frac{C_{qe}^{32}}{\Lambda^2} = -1.04 \times 10^{-9} \text{ GeV}^{-2}$	$\frac{C_{lequ}^{(1)32}}{\Lambda^2} = 0$ $\frac{C_{lequ}^{(3)32}}{\Lambda^2} = 7.24 \times 10^{-11} \text{ GeV}^{-2}$
III	$\frac{C_{lq}^{(1)32}}{\Lambda^2} = -9.96 \times 10^{-10} \text{ GeV}^{-2},$ $\frac{C_{qe}^{32}}{\Lambda^2} = -1.04 \times 10^{-9} \text{ GeV}^{-2}$	$\frac{C_{lequ}^{(1)}}{\Lambda^2} = -9.27 \times 10^{-10} \text{ GeV}^{-2},$ $\frac{C_{lequ}^{(3)32}}{\Lambda^2} = 7.24 \times 10^{-11} \text{ GeV}^{-2}$

Table 7: Different benchmark cases of coupling combinations to study optimal correlations and separability from the SM.

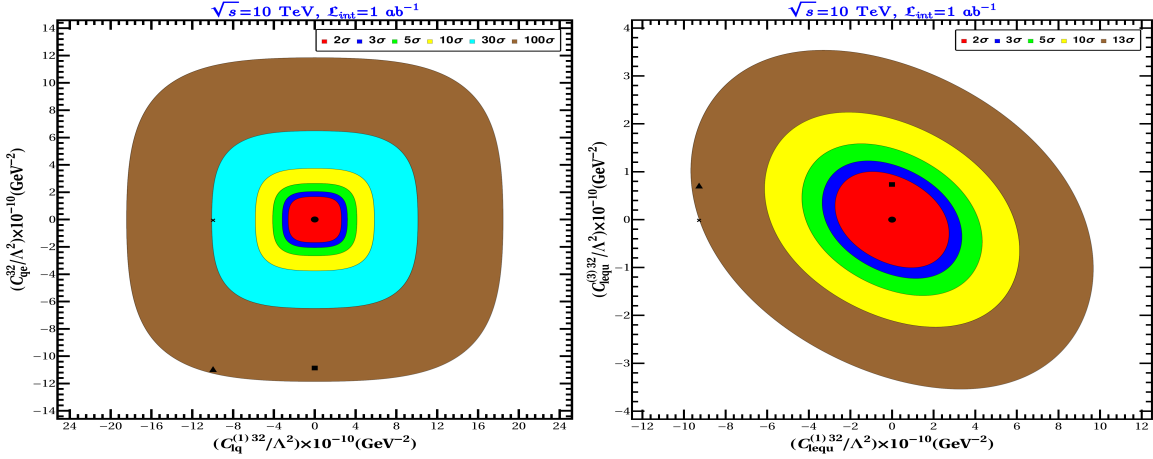


Figure 9: Separation of different cases mentioned in Table 7; left: $C_{lq}^{(1)32}/\Lambda^2 - C_{qe}^{32}/\Lambda^2$ plane, right: $C_{lequ}^{(1)32}/\Lambda^2 - C_{lequ}^{(3)32}/\Lambda^2$ plane. The representative points related to case-I, case-II, and case-III are denoted by cross (\times), triangle (\triangle), and square (\square). The ‘base model’ SM is represented by the dot (\bullet). Different $n\sigma$ regions are presented in the inset of the figures.

Case-I, Case-II, and Case-III are 28.18σ (24.93σ), 76.97σ (1.18σ), and 87.34σ (23σ) away from SM respectively, so that the distinction of vector operators is comparatively easier than the scalar and tensor operators once we adhere to the benchmark points respecting flavor constraints. Estimated values of vector, scalar, and tensor couplings are noted in Table 8 for different CM energies and luminosities at 5σ separation. To achieve the 5σ separation for tensor operator with current flavor bound, we require 18 ab^{-1} integrated luminosity for 10 TeV CM energy.

Couplings (GeV ⁻²)	$\sqrt{s} = 10$ TeV, $\mathfrak{L}_{\text{int}}=1$ ab ⁻¹	$\sqrt{s} = 10$ TeV, $\mathfrak{L}_{\text{int}}=10$ ab ⁻¹	$\sqrt{s} = 30$ TeV, $\mathfrak{L}_{\text{int}}=1$ ab ⁻¹	$\sqrt{s} = 30$ TeV, $\mathfrak{L}_{\text{int}}=10$ ab ⁻¹
$C_{lq}^{(1)32}/\Lambda^2$	-4.13×10^{-10}	-3.14×10^{-10}	-7.92×10^{-11}	-4.45×10^{-11}
$C_{lequ}^{(1)32}/\Lambda^2$	-7.88×10^{-11}	-2.33×10^{-11}	-7.88×10^{-11}	-4.43×10^{-11}
$C_{lequ}^{(3)32}/\Lambda^2$	14.93×10^{-11}	8.39×10^{-11}	2.81×10^{-11}	1.58×10^{-11}

Table 8: Values of vector ($C_{lq}^{(1)32}/\Lambda^2$), scalar ($C_{lequ}^{(1)32}/\Lambda^2$), and tensor ($C_{lequ}^{(3)32}/\Lambda^2$) couplings at different CM energies and luminosities at 5σ separation.

6 Sensitivity of "flavor-relaxed" ($C_{lequ}^{(1)32}/\Lambda^2$) at the 500 GeV ILC

As seen from Table 2, the simultaneous fit on the scalar-mediated WC from $3 \rightarrow 2$ transition observables provides a less stringent bound compared to the other cases or when we combine all the flavor-violating observables together. Specifically, the order of $C_{lequ}^{(1)32}/\Lambda^2$ from $3 \rightarrow 2$ transition observables is $\sim 10^{-7}$ GeV⁻², whereas the best fit value from combining all the flavor-violating observables is of the order $\sim 10^{-9}$ GeV⁻². Therefore, $C_{lequ}^{(1)32}/\Lambda^2$ can be probed at a much lower CM energy preferable at the electron-positron machine such as International Linear Collider (ILC) [105, 106]. In this segment, we provide analyse probing this operator at the ILC with $\sqrt{s} = 500$ GeV. At this CM energy, the outgoing particles are less boosted and hence collimation of decay products, as observed at multi-TeV colliders, is less likely to occur. Hence, an untagged di-jet analysis in such scenario will not be much helpful to segregate the signal processes from the huge two jet background possibilities. This motivates us to revert back to the traditional channels emerging from the heavy particle decay.

For tc production, we choose the signal process $t(bW(\ell\nu))c$ *i.e.* di-jet (one b -tagged, other c -tagged) plus one lepton with missing energy (\cancel{E}). The relevant non-interfering SM background processes are $W(\ell\nu)W(jj)$, $t(bW(\ell\nu))\bar{t}(\bar{b}W(\ell\nu))$ and $W(\ell\nu)jj$. Here, j corresponds to light jets (u, d, s), c -jets and b -jets collectively. Due to the large uncertainty in c and b tagging, miss-tagging of light jets and c -jets as b -jets and light jets and b -jets as c -jets should be taken into account. The $t\bar{t}$ background contributes as a result of a missing lepton and miss-tagging of b from top decay as c . The event simulation is done in similar lines with Section 4.2.1. The b and c tagging are done using *ILCgen Delphes* card based on ILC Snowmass projection [106]. The b and c tagging efficiencies are 0.702 and 0.315 respectively⁸. The invariant mass of the outgoing products turn out to be an important discriminator of the signal and background process, as shown in figure 10. The jets (b and c) in WW and Wjj are expected to peak at the W pole which isn't the case for tc and $t\bar{t}$. Similarly, the top decay products, $b\bar{\ell}$ are expected to peak around 100 GeV, taking into account the energy carried away by the invisible neutrino. Finally the c -jet from the signal process results from a contact interaction, in contrary to WW and $t\bar{t}$, where it is produced in W decay; thus the invariant mass between c and ℓ/b for the signal is expected to be

⁸The mistagging rates of $b(c)$ jet as light jets and $c(b)$ jet are 0.0613(0.0168) and 0.289(0.105) respectively.

shifted more towards the CM energy, compared to the backgrounds. This works as an important discriminant in segregating the signal from $t\bar{t}$ background. The event cross-section after subsequent cutflow is shown in Table 9. After all the kinematical cuts, 5σ significance for this specific final state signal can be achieved at 10 fb^{-1} luminosity with $\sqrt{s} = 500 \text{ GeV}$ at the ILC.

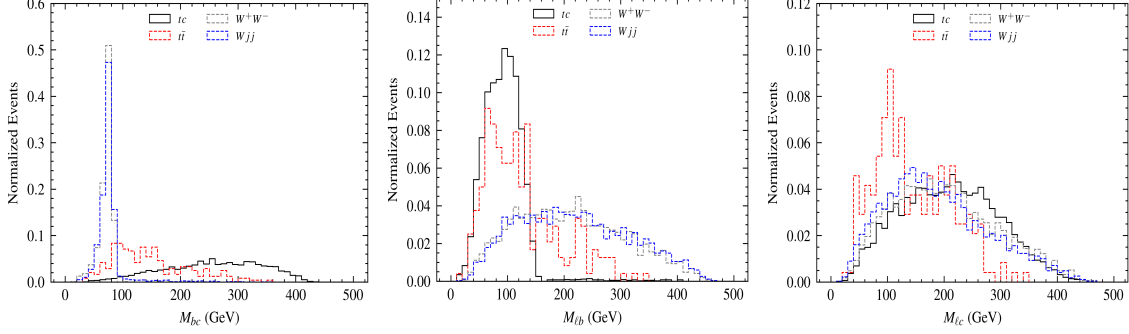


Figure 10: Invariant mass distributions corresponding to ℓbc signal for signal and background processes at ILC 500 GeV run. For the signal process, we choose the benchmark: $C_{lequ}^{(1)32}/\Lambda^2 = 1.79 \times 10^{-7} \text{ GeV}^{-2}$, based on the flavor constraint obtained from Table 2.

Processes	$\sigma(\mathcal{S})$ $(N_\ell, N_b, N_c) = (1, 1, 1)$	$\sigma(\mathcal{C}_1)$ $M_{bc} > 100 \text{ GeV}$	$\sigma(\mathcal{C}_2)$ $M_{lb} < 150 \text{ GeV}$	$\sigma(\mathcal{C}_3)$ $M_{lc} > 150 \text{ GeV}$
tc	6296	6057	5975	4413
$t\bar{t}$	1366	979	723	330
WW	18899	28	7	0
Wjj	17317	821	291	110

Table 9: Signal and background events following each cut ($\mathcal{S}, \mathcal{C}_1, \mathcal{C}_2, \mathcal{C}_3$) at the ILC with 500 GeV CM energy and 1 ab^{-1} luminosity. Here, N_ℓ , N_b and N_c refer to the number of leptons, b -tagged jets and c -tagged jets respectively. M_{ij} is the invariant mass of the i^{th} and j^{th} particles. For the signal process, we choose benchmark value $C_{lequ}^{(1)32}/\Lambda^2 = 1.79 \times 10^{-7} \text{ GeV}^{-2}$.

Subsequently, we analyze the optimal sensitivity of $C_{lequ}^{(1)32}/\Lambda^2$ with $\sqrt{s} = 500 \text{ GeV}$ and $\mathcal{L}_{\text{int}} = 1 \text{ ab}^{-1}$ at the ILC. The optimal $\Delta\chi^2$ variation with $C_{lequ}^{(1)32}/\Lambda^2$ is shown in the figure 11 and compared with the flavor data. The figure demonstrates that the optimal uncertainty is much tighter than the flavor uncertainty in this case.

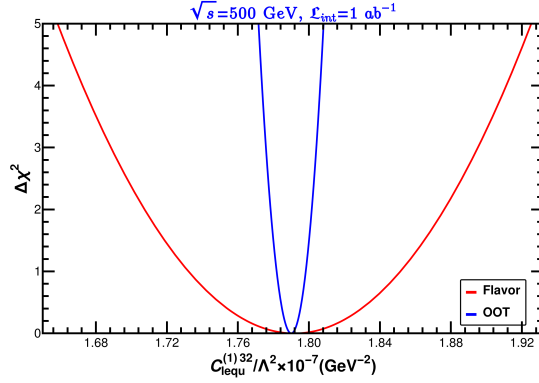


Figure 11: $\Delta\chi^2$ variation in red (blue) for flavor (OOT) as a function of dimension-six scalar mediated effective coupling at benchmark $C_{lequ}^{(1)32}/\Lambda^2 = 1.79 \times 10^{-7} \text{ GeV}^{-2}$ based on the flavor constraint obtained from Table 2.

7 Summary and Conclusion

In this paper, we have explored the SMEFT operators that contribute to tc ($\bar{t}c + t\bar{c}$) production at colliders. The most significant contribution arises from the quark flavor violating four-Fermi operators. The other operator which provides modification to Ztc vertex has much less contribution at high CM energy and have thus been ignored in this analysis. Such four-Fermi operators contribute significantly to low energy flavor dependent processes and are thus heavily constrained by them. We study all such FCNC and FCCC processes including $b \rightarrow s(d)$ transitions, $P \rightarrow \ell\nu$, $K_L \rightarrow \mu\mu$, $B - \bar{B}$ mixing, top decays etc., to constrain the four-Fermi SMEFT operators. The most stringent bound arises on the tensor operator, having $C_{lequ}^{(3)32}/\Lambda^2 \sim 10^{-11} \text{ GeV}^{-2}$, followed by a conservative limit on scalar operator $C_{lequ}^{(1)32}/\Lambda^2 \sim 10^{-9} \text{ GeV}^{-2}$, and vector operator $C_{lq}^{(1)32}/\Lambda^2 \sim 10^{-9} \text{ GeV}^{-2}$ (Although, the order is same, scalar operators is slightly more constrained than vector operator). We also predict observational sensitivities of the processes like $K_L \rightarrow \pi_0 \ell\ell$, $D_0 \rightarrow \mu\mu$, $t \rightarrow c\ell\ell$ and $t \rightarrow c\gamma$ from the obtained limits and show that they are consistent with the existing upper bounds.

Using these constraints, we have examined the future probe of these SMEFT operators at multi-TeV moun collider through tc ($\bar{t}c + t\bar{c}$) production. The required CM energy is 10 TeV where the production cross-section is of the order of fb, respecting EFT constraint $\Lambda > \sqrt{s}$. Given the high CM energy, the process basically yields di-jet final state (a ‘top’ jet and a ‘charm’ jet) with no leptons stemming from the top decay. There is apparently a little chance of tagging them as well, which incorporates several SM backgrounds. There exists very little number of variables at disposal to segregate the signal from background, amongst which invariant di-jet mass and invariant mass of the heavy jet plays an important role to achieve a satisfactory signal significance for vector and scalar operator benchmarks in particular, at high luminosity 1 ab^{-1} .

Using OOT, we have determined the optimal uncertainties of the vector, scalar and tensor type effective couplings at the benchmarks respecting flavor constraints. We see that at 10 TeV CM energy muon collider with 1 ab^{-1} integrated luminosity optimal uncertainty of the effective C/Λ^2 is better than the flavor uncertainty. Relative contribution between NP signal and non-interfering SM background play an important role in NP estimation, the less the background, the better the estimation. The dependence of the uncertainty on the CM energy and luminosity has also been compared and the advantages of CM energy to estimate optimal uncertainty pertaining to the EFT limit is discussed. Considering SM as a base model, distinction of different operators from the SM has also been studied. We have observed that at 10 TeV CM energy, 30 fb^{-1} luminosity is required to segregate (at 5σ level) vector ($\mathcal{O}_{lq}^{(1)}$) operators from the SM, whereas for scalar ($\mathcal{O}_{lequ}^{(1)}$) and tensor ($\mathcal{O}_{lequ}^{(3)}$) operators we need 40 fb^{-1} and 18 ab^{-1} integrated luminosity, respectively, after obeying flavor constraints. However, in a more optimistic case of less stringent scalar operator having $C_{lequ}^{(1)32}/\Lambda^2 \sim 10^{-7} \text{ GeV}^{-2}$, 5σ segregation can be achieved at 500 GeV CM energy and 10 fb^{-1} luminosity at the ILC.

Acknowledgments

Sahabub Jahedi would like to thank Lipika Kolay and Ipsita Saha for useful discussions.

A Loop function for $B_q - \bar{B}_q$ mixings and amplitudes of $t \rightarrow b\ell\nu$

- Loop function:

$$\text{DiscB}(a, b, c) = \frac{1}{a} \lambda(a, b^2, c^2) \text{Log} \left[\frac{-a + b^2 + c^2 + \sqrt{\lambda(a, b^2, c^2)}}{2bc} \right], \quad (\text{A.1})$$

where $\lambda(x, y, z) = x^2 + y^2 + z^2 - 2(xy + yz + zx)$.

- $t \rightarrow b\ell\nu_\ell$ decay: The SM and BSM contributions to the $t(p) \rightarrow b(k)\ell(k_1)\nu(k_2)$ decay amplitude are written as

$$\begin{aligned} \mathcal{M}_{\text{SM}}^t &= \frac{g^2}{2\sqrt{2}((q^2 - m_W^2) + i\Gamma_W m_W)} \bar{u}(k)\gamma^\mu P_L u(p) \bar{u}(k_2)\gamma_\mu P_L v(k_1), \\ \mathcal{M}_{\text{NP}}^t &= -\frac{C_{lq}^{(3)32}}{\Lambda^2} \bar{u}(k)\gamma^\mu P_L u(p) \bar{u}(k_2)\gamma_\mu P_L v(k_1) \\ &\quad + \frac{C_{lequ}^{(1)32}}{\Lambda^2} (\bar{u}(k_1)P_R v(k_2)) (\bar{v}(p_2)P_R u(p_1)) \\ &\quad + \frac{C_{lequ}^{(3)32}}{\Lambda^2} (\bar{u}(k_1)\sigma^{\mu\nu}P_R v(k_2)) (\bar{v}(p_2)\sigma_{\mu\nu}P_R u(p_1)). \end{aligned} \quad (\text{A.2})$$

B Renormalization Group (RG) Equations

The renormalization group equations of the relevant SMEFT couplings are written as [107–110]

$$\frac{d\tilde{C}_i}{d\ln\mu} = \frac{1}{16\pi^2}\beta_i, \quad (\text{B.1})$$

where $\tilde{C}_i = \left\{ \frac{C_{lq}^{(1)32}}{\Lambda^2}, \frac{C_{lequ}^{(1)32}}{\Lambda^2}, \frac{C_{lequ}^{(3)32}}{\Lambda^2} \right\}$ are the SMEFT coefficients and $\beta_i = \{\beta_{lq}^{(1)32}, \beta_{lequ}^{(1)32}, \beta_{lequ}^{(3)32}\}$ are the respective 1-loop β functions of the SMEFT operators. The β functions are:

$$\begin{aligned}\beta_{lq}^{(1)32} &= g'^2 \frac{C_{lq}^{(1)32}}{\Lambda^2} + [\gamma_q]_{33} \frac{C_{lq}^{(1)32}}{\Lambda^2} + [\gamma_q]_{33} \frac{C_{lq}^{(1)32}}{\Lambda^2}, \\ &= \left(g'^2 + \frac{1}{2} y_t^2 \right) \frac{C_{lq}^{(1)32}}{\Lambda^2};\end{aligned}\tag{B.2}$$

$$\begin{aligned}\beta_{lequ}^{(1)32} &= - \left(\frac{11}{3} g'^2 + 8 g_S^2 \right) \frac{C_{lequ}^{(1)32}}{\Lambda^2} + [\gamma_q]_{33} \frac{C_{lequ}^{(1)32}}{\Lambda^2} + [\gamma_u]_{33} \frac{C_{lequ}^{(1)32}}{\Lambda^2}, \\ &= - \left(\frac{11}{3} g'^2 + 8 g_S^2 - \frac{1}{2} y_t^2 \right) \frac{C_{lequ}^{(1)32}}{\Lambda^2};\end{aligned}\tag{B.3}$$

$$\begin{aligned}\beta_{lequ}^{(3)32} &= - \left(\frac{2}{9} g'^2 - 3 g^2 + \frac{8}{3} g_S^2 \right) \frac{C_{lequ}^{(3)32}}{\Lambda^2} + [\gamma_q]_{33} \frac{C_{lequ}^{(3)32}}{\Lambda^2} + [\gamma_u]_{33} \frac{C_{lequ}^{(3)32}}{\Lambda^2}, \\ &= - \left(\frac{2}{9} g'^2 - 3 g^2 + \frac{8}{3} g_S^2 - \frac{1}{2} y_t^2 \right) \frac{C_{lequ}^{(3)32}}{\Lambda^2};\end{aligned}\tag{B.4}$$

Here, $\gamma_q = \frac{1}{2} (y_u y_u^\dagger + y_d y_d^\dagger)$ and $\gamma_u = (y_u y_u^\dagger)$. We consider, $y_u = y_d = 0$ except for y_t . The RGEs for the SM parameters are noted below:

$$\begin{aligned}\frac{dg}{d \ln \mu} &= \frac{1}{16\pi^2} \left(-\frac{19}{6} g^3 \right), \\ \frac{dg'}{d \ln \mu} &= \frac{1}{16\pi^2} \left(\frac{41}{6} g'^3 \right), \\ \frac{dg_S}{d \ln \mu} &= \frac{1}{16\pi^2} \left(-7 g_S^2 \right), \\ \frac{dy_t}{d \ln \mu} &= \frac{y_t}{16\pi^2} \left(\frac{9}{4} g^2 - \frac{17}{12} g'^2 - 8 g_S^2 + \frac{9}{2} y_t^2 \right).\end{aligned}\tag{B.5}$$

The variation of the dimension-six effective couplings with the renormalization scale (μ) is illustrated in figure 12, with comparisons and validation provided by Wilson [111].

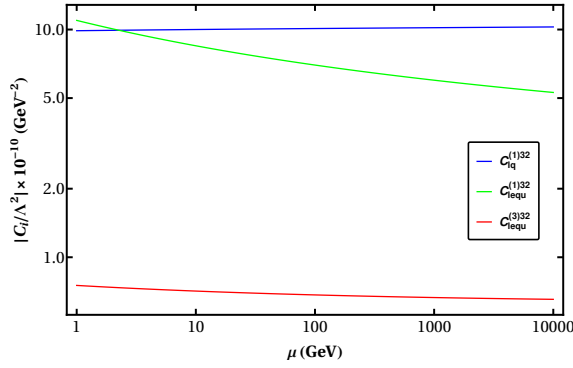


Figure 12: RG running for dimension-six vector ($C_{lq}^{(1)32}/\Lambda^2$), scalar ($C_{lequ}^{(1)32}/\Lambda^2$), and tensor ($C_{lequ}^{(3)32}/\Lambda^2$) couplings with the energy scale (μ).

References

- [1] S. Weinberg, *Baryon and Lepton Nonconserving Processes*, *Phys. Rev. Lett.* **43** (1979) 1566.
- [2] W. Buchmuller and D. Wyler, *Effective Lagrangian Analysis of New Interactions and Flavor Conservation*, *Nucl. Phys. B* **268** (1986) 621.
- [3] B. Grzadkowski, M. Iskrzynski, M. Misiak and J. Rosiek, *Dimension-Six Terms in the Standard Model Lagrangian*, *JHEP* **10** (2010) 085 [[1008.4884](#)].
- [4] L. Lehman, *Extending the Standard Model Effective Field Theory with the Complete Set of Dimension-7 Operators*, *Phys. Rev. D* **90** (2014) 125023 [[1410.4193](#)].
- [5] S. Bhattacharya and J. Wudka, *Dimension-seven operators in the standard model with right handed neutrinos*, *Phys. Rev. D* **94** (2016) 055022 [[1505.05264](#)].
- [6] C. W. Murphy, *Dimension-8 operators in the Standard Model Effective Field Theory*, *JHEP* **10** (2020) 174 [[2005.00059](#)].
- [7] H.-L. Li, Z. Ren, J. Shu, M.-L. Xiao, J.-H. Yu and Y.-H. Zheng, *Complete set of dimension-eight operators in the standard model effective field theory*, *Phys. Rev. D* **104** (2021) 015026 [[2005.00008](#)].
- [8] H. H. Asatrian, H. M. Asatrian, C. Greub and M. Walker, *Two loop virtual corrections to $B \rightarrow X_s l^+ l^-$ in the standard model*, *Phys. Lett. B* **507** (2001) 162 [[hep-ph/0103087](#)].
- [9] H. H. Asatryan, H. M. Asatrian, C. Greub and M. Walker, *Calculation of two loop virtual corrections to $b \rightarrow s l^+ l^-$ in the standard model*, *Phys. Rev. D* **65** (2002) 074004 [[hep-ph/0109140](#)].
- [10] H. M. Asatrian, K. Bieri, C. Greub and M. Walker, *Virtual corrections and bremsstrahlung corrections to $b \rightarrow d l^+ l^-$ in the standard model*, *Phys. Rev. D* **69** (2004) 074007 [[hep-ph/0312063](#)].
- [11] R. Aoude, T. Hurth, S. Renner and W. Shepherd, *The impact of flavour data on global fits of the MFV SMEFT*, *JHEP* **12** (2020) 113 [[2003.05432](#)].
- [12] S. Bismann, C. Grunwald, G. Hiller and K. Kröninger, *Top and Beauty synergies in SMEFT-fits at present and future colliders*, *JHEP* **06** (2021) 010 [[2012.10456](#)].

- [13] J. Alda, J. Guasch and S. Penaranda, *Anomalies in B mesons decays: a phenomenological approach*, *Eur. Phys. J. Plus* **137** (2022) 217 [[2012.14799](#)].
- [14] S. Bruggisser, R. Schäfer, D. van Dyk and S. Westhoff, *The Flavor of UV Physics*, *JHEP* **05** (2021) 257 [[2101.07273](#)].
- [15] C. Grunwald, G. Hiller, K. Kröninger and L. Nollen, *More Synergies from Beauty, Top, Z and Drell-Yan Measurements in SMEFT*, [2304.12837](#).
- [16] M. I. Ali, U. Chattopadhyay, N. Rajeev and J. Roy, *SMEFT analysis of charged lepton flavor violating B-meson decays*, [2312.05071](#).
- [17] M. Chala, J. Santiago and M. Spannowsky, *Constraining four-fermion operators using rare top decays*, *JHEP* **04** (2019) 014 [[1809.09624](#)].
- [18] S. Bibmann, J. Erdmann, C. Grunwald, G. Hiller and K. Kröninger, *Constraining top-quark couplings combining top-quark and B decay observables*, *Eur. Phys. J. C* **80** (2020) 136 [[1909.13632](#)].
- [19] W. Altmannshofer, S. Gori, B. V. Lehmann and J. Zuo, *UV physics from IR features: New prospects from top flavor violation*, *Phys. Rev. D* **107** (2023) 095025 [[2303.00781](#)].
- [20] K. M. Black et al., *Muon Collider Forum Report*, [2209.01318](#).
- [21] V. Shiltsev and F. Zimmermann, *Modern and Future Colliders*, *Rev. Mod. Phys.* **93** (2021) 015006 [[2003.09084](#)].
- [22] S. Bar-Shalom, G. Eilam, A. Soni and J. Wudka, *Probing the flavor changing tc vertex via tree level processes: $e^+e^- \rightarrow t$ anti- c electron-neutrino anti-electron-neutrino, t anti- c e^+e^- and $t \rightarrow c$ W^+W^-* , *Phys. Rev. Lett.* **79** (1997) 1217 [[hep-ph/9703221](#)].
- [23] S. Bar-Shalom, G. Eilam, A. Soni and J. Wudka, *Implications of a $W^+W^- (ZZ) - \text{Higgs} - t$ anti- c interaction for $e^+e^- \rightarrow t$ anti- c electron-neutrino anti-electron-neutrino, t anti- c e^+e^- , t anti- c Z and for $t \rightarrow c$ W^+W^- , c ZZ in a two Higgs doublet model*, *Phys. Rev. D* **57** (1998) 2957 [[hep-ph/9708358](#)].
- [24] S. Bar-Shalom and J. Wudka, *Flavor changing single top quark production channels at e^+e^- colliders in the effective Lagrangian description*, *Phys. Rev. D* **60** (1999) 094016 [[hep-ph/9905407](#)].
- [25] S. Sun, Q.-S. Yan, X. Zhao and Z. Zhao, *Constraining rare B decays by $\mu^+\mu^- \rightarrow tc$ at future lepton colliders*, *Phys. Rev. D* **108** (2023) 075016 [[2302.01143](#)].
- [26] D. Atwood and A. Soni, *Analysis for magnetic moment and electric dipole moment form-factors of the top quark via $e^+e^- \rightarrow t\bar{t}$* , *Phys. Rev. D* **45** (1992) 2405.
- [27] M. Davier, L. Duflot, F. Le Diberder and A. Rouge, *The Optimal method for the measurement of tau polarization*, *Phys. Lett. B* **306** (1993) 411.
- [28] M. Diehl and O. Nachtmann, *Optimal observables for the measurement of three gauge boson couplings in $e^+e^- \rightarrow W^+W^-$* , *Z. Phys. C* **62** (1994) 397.
- [29] J. F. Gunion, B. Grzadkowski and X.-G. He, *Determining the $t\bar{t}$ and ZZ couplings of a neutral Higgs boson of arbitrary CP nature at the NLC*, *Phys. Rev. Lett.* **77** (1996) 5172 [[hep-ph/9605326](#)].
- [30] K. Hagiwara, S. Ishihara, J. Kamoshita and B. A. Kniehl, *Prospects of measuring general Higgs couplings at e^+e^- linear colliders*, *Eur. Phys. J. C* **14** (2000) 457 [[hep-ph/0002043](#)].

- [31] S. Dutta, K. Hagiwara and Y. Matsumoto, *Measuring the Higgs-Vector boson Couplings at Linear e^+e^- Collider*, *Phys. Rev. D* **78** (2008) 115016 [[0808.0477](#)].
- [32] B. Grzadkowski, Z. Hioki, K. Ohkuma and J. Wudka, *Probing anomalous top quark couplings induced by dimension-six operators at photon colliders*, *Nucl. Phys. B* **689** (2004) 108 [[hep-ph/0310159](#)].
- [33] B. Grzadkowski, Z. Hioki, K. Ohkuma and J. Wudka, *Optimal-observable analysis of possible new physics using the b quark in $\gamma\gamma \rightarrow t\bar{t} \rightarrow bX$* , *Phys. Lett. B* **593** (2004) 189 [[hep-ph/0403174](#)].
- [34] B. Grzadkowski, Z. Hioki, K. Ohkuma and J. Wudka, *Optimal beam polarizations for new-physics search through $\gamma\gamma \rightarrow t\bar{t} \rightarrow lX/bX$* , *JHEP* **11** (2005) 029 [[hep-ph/0508183](#)].
- [35] S. Bhattacharya, S. Jahedi and J. Wudka, *Optimal determination of New Physics couplings with dominant and subdominant Standard Model contribution*, [2301.07721](#).
- [36] J. F. Gunion and J. Pliszka, *Determining the relative size of the CP even and CP odd Higgs boson couplings to a fermion at the LHC*, *Phys. Lett. B* **444** (1998) 136 [[hep-ph/9809306](#)].
- [37] Q.-H. Cao and J. Wudka, *Search for new physics via single top production at TeV energy $e\gamma$ colliders*, *Phys. Rev. D* **74** (2006) 094015 [[hep-ph/0608331](#)].
- [38] Z. Hioki, T. Konishi and K. Ohkuma, *Studying possible CP-violating Higgs couplings through top-quark pair productions at muon colliders*, *JHEP* **07** (2007) 082 [[0706.4346](#)].
- [39] S. Bhattacharya, S. Jahedi and J. Wudka, *Probing heavy charged fermions at e^+e^- collider using the optimal observable technique*, *JHEP* **05** (2022) 009 [[2106.02846](#)].
- [40] S. Jahedi and J. Lahiri, *Probing anomalous $ZZ\gamma$ and $Z\gamma\gamma$ couplings at the e^+e^- colliders using optimal observable technique*, *JHEP* **04** (2023) 085 [[2212.05121](#)].
- [41] S. Jahedi, *Optimal estimation of Dimension-8 Neutral Triple Gauge Couplings at e^+e^- Colliders*, [2305.11266](#).
- [42] C. Bobeth, M. Misiak and J. Urban, *Photonic penguins at two loops and m_t dependence of $BR[B \rightarrow X_s l^+ l^-]$* , *Nucl. Phys. B* **574** (2000) 291 [[hep-ph/9910220](#)].
- [43] W. Altmannshofer, P. Ball, A. Bharucha, A. J. Buras, D. M. Straub and M. Wick, *Symmetries and Asymmetries of $B \rightarrow K^* \mu^+ \mu^-$ Decays in the Standard Model and Beyond*, *JHEP* **01** (2009) 019 [[0811.1214](#)].
- [44] J. Aebischer, A. Crivellin, M. Fael and C. Greub, *Matching of gauge invariant dimension-six operators for $b \rightarrow s$ and $b \rightarrow c$ transitions*, *JHEP* **05** (2016) 037 [[1512.02830](#)].
- [45] S. Descotes-Genon, J. Matias, M. Ramon and J. Virto, *Implications from clean observables for the binned analysis of $B \rightarrow K^* \mu^+ \mu^-$ at large recoil*, *JHEP* **01** (2013) 048 [[1207.2753](#)].
- [46] S. Descotes-Genon, T. Hurth, J. Matias and J. Virto, *Optimizing the basis of $B \rightarrow K^* l l$ observables in the full kinematic range*, *JHEP* **05** (2013) 137 [[1303.5794](#)].
- [47] R. R. Horgan, Z. Liu, S. Meinel and M. Wingate, *Calculation of $B^0 \rightarrow K^{*0} \mu^+ \mu^-$ and $B_s^0 \rightarrow \phi \mu^+ \mu^-$ observables using form factors from lattice QCD*, *Phys. Rev. Lett.* **112** (2014) 212003 [[1310.3887](#)].
- [48] A. Bharucha, D. M. Straub and R. Zwicky, *$B \rightarrow V \ell^+ \ell^-$ in the Standard Model from light-cone sum rules*, *JHEP* **08** (2016) 098 [[1503.05534](#)].
- [49] A. Biswas, S. Nandi, S. K. Patra and I. Ray, *New physics in $b \rightarrow \ell\ell$ decays with complex wilson coefficients*, *Nucl. Phys. B* **969** (2021) 115479 [[2004.14687](#)].

- [50] CDF collaboration, *Measurements of the Angular Distributions in the Decays $B \rightarrow K^{(*)}\mu^+\mu^-$ at CDF*, *Phys. Rev. Lett.* **108** (2012) 081807 [[1108.0695](#)].
- [51] LHCb collaboration, *Measurement of the CP asymmetry in $B^+ \rightarrow K^+\mu^+\mu^-$ decays*, *Phys. Rev. Lett.* **111** (2013) 151801 [[1308.1340](#)].
- [52] LHCb collaboration, *Differential branching fractions and isospin asymmetries of $B \rightarrow K^{(*)}\mu^+\mu^-$ decays*, *JHEP* **06** (2014) 133 [[1403.8044](#)].
- [53] LHCb collaboration, *Test of lepton universality using $B^+ \rightarrow K^+\ell^+\ell^-$ decays*, *Phys. Rev. Lett.* **113** (2014) 151601 [[1406.6482](#)].
- [54] LHCb collaboration, *Angular analysis of the $B^0 \rightarrow K^{*0}\mu^+\mu^-$ decay using 3 fb^{-1} of integrated luminosity*, *JHEP* **02** (2016) 104 [[1512.04442](#)].
- [55] BELLE collaboration, *Lepton-Flavor-Dependent Angular Analysis of $B \rightarrow K^*\ell^+\ell^-$* , *Phys. Rev. Lett.* **118** (2017) 111801 [[1612.05014](#)].
- [56] CMS collaboration, *Measurement of angular parameters from the decay $B^0 \rightarrow K^{*0}\mu^+\mu^-$ in proton-proton collisions at $\sqrt{s} = 8\text{ TeV}$* , *Phys. Lett. B* **781** (2018) 517 [[1710.02846](#)].
- [57] ATLAS collaboration, *Angular analysis of $B_d^0 \rightarrow K^*\mu^+\mu^-$ decays in pp collisions at $\sqrt{s} = 8\text{ TeV}$ with the ATLAS detector*, *JHEP* **10** (2018) 047 [[1805.04000](#)].
- [58] LHCb collaboration, *Angular Analysis of the $B^+ \rightarrow K^{*+}\mu^+\mu^-$ Decay*, *Phys. Rev. Lett.* **126** (2021) 161802 [[2012.13241](#)].
- [59] LHCb collaboration, *Branching Fraction Measurements of the Rare $B_s^0 \rightarrow \phi\mu^+\mu^-$ and $B_s^0 \rightarrow f_2'(1525)\mu^+\mu^-$ Decays*, *Phys. Rev. Lett.* **127** (2021) 151801 [[2105.14007](#)].
- [60] LHCb collaboration, *Test of lepton universality in $b \rightarrow s\ell^+\ell^-$ decays*, *Phys. Rev. Lett.* **131** (2023) 051803 [[2212.09152](#)].
- [61] LHCb collaboration, *Measurement of lepton universality parameters in $B^+ \rightarrow K^+\ell^+\ell^-$ and $B^0 \rightarrow K^{*0}\ell^+\ell^-$ decays*, *Phys. Rev. D* **108** (2023) 032002 [[2212.09153](#)].
- [62] A. V. Rusov, *Probing New Physics in $b \rightarrow d$ transitions*, *JHEP* **07** (2020) 158 [[1911.12819](#)].
- [63] R. Bause, H. Gisbert, M. Golz and G. Hiller, *Model-independent analysis of $b \rightarrow d$ processes*, *Eur. Phys. J. C* **83** (2023) 419 [[2209.04457](#)].
- [64] G. Isidori and R. Unterdorfer, *On the short distance constraints from $K(L,S) \rightarrow \mu^+\mu^-$* , *JHEP* **01** (2004) 009 [[hep-ph/0311084](#)].
- [65] V. Chobanova, G. D'Ambrosio, T. Kitahara, M. Lucio Martinez, D. Martinez Santos, I. S. Fernandez et al., *Probing SUSY effects in $K_S^0 \rightarrow \mu^+\mu^-$* , *JHEP* **05** (2018) 024 [[1711.11030](#)].
- [66] G. Ecker and A. Pich, *The Longitudinal muon polarization in $K(L) \rightarrow \mu^+\mu^-$* , *Nucl. Phys. B* **366** (1991) 189.
- [67] G. D'Ambrosio, A. M. Iyer, F. Mahmoudi and S. Neshatpour, *Anatomy of kaon decays and prospects for lepton flavour universality violation*, *JHEP* **09** (2022) 148 [[2206.14748](#)].
- [68] J. S. Hagelin, *Mass Mixing and CP Violation in the $B^0 - \bar{B}^0$ system*, *Nucl. Phys. B* **193** (1981) 123.
- [69] A. Ali and C. Jarlskog, *Signatures of $B(s)0 - \bar{B}(s)0$ Mixings in $p\bar{p}$ and e^+e^- Collisions*, *Phys. Lett. B* **144** (1984) 266.
- [70] L.-L. Chau and W.-Y. Keung, *Implications From the b Decay Measurements*, *Phys. Rev. D* **29** (1984) 592.

- [71] FLAVOUR LATTICE AVERAGING GROUP (FLAG) collaboration, *FLAG Review 2021*, [*Eur. Phys. J. C* **82** \(2022\) 869 \[2111.09849\]](#).
- [72] C. Gay, *B mixing*, [*Ann. Rev. Nucl. Part. Sci.* **50** \(2000\) 577 \[hep-ex/0103016\]](#).
- [73] D. Becirevic, N. Kosnik, F. Mescia and E. Schneider, *Complementarity of the constraints on New Physics from $B_s \rightarrow \mu^+ \mu^-$ and from $B \rightarrow K l^+ l^-$ decays*, [*Phys. Rev. D* **86** \(2012\) 034034 \[1205.5811\]](#).
- [74] CMS, LHCb collaboration, *Observation of the rare $B_s^0 \rightarrow \mu^+ \mu^-$ decay from the combined analysis of CMS and LHCb data*, [*Nature* **522** \(2015\) 68 \[1411.4413\]](#).
- [75] V. Cirigliano, G. Ecker, H. Neufeld, A. Pich and J. Portoles, *Kaon Decays in the Standard Model*, [*Rev. Mod. Phys.* **84** \(2012\) 399 \[1107.6001\]](#).
- [76] G. Buchalla and A. J. Buras, *The rare decays $K \rightarrow \pi \nu \bar{\nu}$, $B \rightarrow X \nu \bar{\nu}$ and $B \rightarrow l^+ l^-$: An Update*, [*Nucl. Phys. B* **548** \(1999\) 309 \[hep-ph/9901288\]](#).
- [77] G. Buchalla, A. J. Buras and M. E. Lautenbacher, *Weak decays beyond leading logarithms*, [*Rev. Mod. Phys.* **68** \(1996\) 1125 \[hep-ph/9512380\]](#).
- [78] L.-S. Geng, J. M. Camalich and R.-X. Shi, *New physics in $s \rightarrow d$ semileptonic transitions: rare hyperon vs. kaon decays*, [*JHEP* **02** \(2022\) 178 \[2112.11979\]](#).
- [79] A. Buras, *Gauge Theory of Weak Decays*. Cambridge University Press, 6, 2020, [10.1017/9781139524100](#).
- [80] PARTICLE DATA GROUP collaboration, *Review of Particle Physics*, [*PTEP* **2022** \(2022\) 083C01](#).
- [81] I. Ray and S. Nandi, *Test of new physics effects in $\bar{B} \rightarrow (D^{(*)}, \pi) \ell^- \bar{\nu}_\ell$ decays with heavy and light leptons*, [2305.11855](#).
- [82] Y. Sakaki, M. Tanaka, A. Tayduganov and R. Watanabe, *Testing leptoquark models in $\bar{B} \rightarrow D^{(*)} \tau \bar{\nu}$* , [*Phys. Rev. D* **88** \(2013\) 094012 \[1309.0301\]](#).
- [83] S. Bhattacharya, S. Nandi and S. Kumar Patra, *$b \rightarrow c \tau \nu_\tau$ Decays: a catalogue to compare, constrain, and correlate new physics effects*, [*Eur. Phys. J. C* **79** \(2019\) 268 \[1805.08222\]](#).
- [84] Z.-R. Huang, Y. Li, C.-D. Lu, M. A. Paracha and C. Wang, *Footprints of New Physics in $b \rightarrow c \tau \nu$ Transitions*, [*Phys. Rev. D* **98** \(2018\) 095018 \[1808.03565\]](#).
- [85] M. Fedele, M. Blanke, A. Crivellin, S. Iguro, U. Nierste, S. Simula et al., *Discriminating $B \rightarrow D^* \ell \nu$ form factors via polarization observables and asymmetries*, [*Phys. Rev. D* **108** \(2023\) 055037 \[2305.15457\]](#).
- [86] D. Bečirević, F. Jaffredo, A. Peñuelas and O. Sumensari, *New Physics effects in leptonic and semileptonic decays*, [*JHEP* **05** \(2021\) 175 \[2012.09872\]](#).
- [87] ATLAS collaboration, *Search for flavour-changing neutral current top-quark decays $t \rightarrow q Z$ in proton-proton collisions at $\sqrt{s} = 13$ TeV with the ATLAS detector*, [*JHEP* **07** \(2018\) 176 \[1803.09923\]](#).
- [88] G. Ecker, A. Pich and E. de Rafael, *Radiative Kaon Decays and CP Violation in Chiral Perturbation Theory*, [*Nucl. Phys. B* **303** \(1988\) 665](#).
- [89] G. Ecker, A. Pich and E. de Rafael, *$K \rightarrow \pi$ Lepton+ Lepton- Decays in the Effective Chiral Lagrangian of the Standard Model*, [*Nucl. Phys. B* **291** \(1987\) 692](#).

- [90] E. Golowich, J. Hewett, S. Pakvasa and A. A. Petrov, *Relating $D0$ -anti- $D0$ Mixing and $D0 \rightarrow l^+ l^-$ with New Physics*, *Phys. Rev. D* **79** (2009) 114030 [[0903.2830](#)].
- [91] KTeV collaboration, *Search for the rare decay $K(L) \rightarrow \pi^0 e^+ e^-$* , *Phys. Rev. Lett.* **93** (2004) 021805 [[hep-ex/0309072](#)].
- [92] KTeV collaboration, *Search for the Decay $K_L \rightarrow \pi^0 \mu^+ \mu^-$* , *Phys. Rev. Lett.* **84** (2000) 5279 [[hep-ex/0001006](#)].
- [93] LHCb collaboration, *Search for Rare Decays of $D0$ Mesons into Two Muons*, *Phys. Rev. Lett.* **131** (2023) 041804 [[2212.11203](#)].
- [94] ATLAS collaboration, *Search for flavour-changing neutral currents in processes with one top quark and a photon using 81 fb^{-1} of pp collisions at $\sqrt{s} = 13 \text{ TeV}$ with the ATLAS experiment*, *Phys. Lett. B* **800** (2020) 135082 [[1908.08461](#)].
- [95] J. Duan, Y. Gao, C.-Y. Ji, S. Sun, Y. Yao and Y.-L. Zhang, *Resonant electric probe to axionic dark matter*, *Phys. Rev. D* **107** (2023) 015019 [[2206.13543](#)].
- [96] J. Alwall, R. Frederix, S. Frixione, V. Hirschi, F. Maltoni, O. Mattelaer et al., *The automated computation of tree-level and next-to-leading order differential cross sections, and their matching to parton shower simulations*, *JHEP* **07** (2014) 079 [[1405.0301](#)].
- [97] N. D. Christensen and C. Duhr, *FeynRules - Feynman rules made easy*, *Comput. Phys. Commun.* **180** (2009) 1614 [[0806.4194](#)].
- [98] T. Sjöstrand, S. Ask, J. R. Christiansen, R. Corke, N. Desai, P. Ilten et al., *An introduction to PYTHIA 8.2*, *Comput. Phys. Commun.* **191** (2015) 159 [[1410.3012](#)].
- [99] DELPHES 3 collaboration, *DELPHES 3, A modular framework for fast simulation of a generic collider experiment*, *JHEP* **02** (2014) 057 [[1307.6346](#)].
- [100] M. Cacciari, G. P. Salam and G. Soyez, *FastJet User Manual*, *Eur. Phys. J. C* **72** (2012) 1896 [[1111.6097](#)].
- [101] M. Cacciari, G. P. Salam and G. Soyez, *The anti- k_t jet clustering algorithm*, *JHEP* **04** (2008) 063 [[0802.1189](#)].
- [102] ATLAS collaboration, *Performance and Calibration of the JetFitterCharm Algorithm for c -Jet Identification*, .
- [103] CMS collaboration, *Identification of c -quark jets at the CMS experiment*, .
- [104] S. Bhattacharya, S. Jahedi, J. Lahiri and J. Wudka, *Optimal New Physics estimation in presence of Standard Model backgrounds*, [2312.12514](#).
- [105] *The International Linear Collider Technical Design Report - Volume 1: Executive Summary*, [1306.6327](#).
- [106] ILC INTERNATIONAL DEVELOPMENT TEAM collaboration, *The International Linear Collider: Report to Snowmass 2021*, [2203.07622](#).
- [107] E. E. Jenkins, A. V. Manohar and M. Trott, *Renormalization Group Evolution of the Standard Model Dimension Six Operators I: Formalism and λ Dependence*, *JHEP* **10** (2013) 087 [[1308.2627](#)].
- [108] E. E. Jenkins, A. V. Manohar and M. Trott, *Renormalization Group Evolution of the Standard Model Dimension Six Operators II: Yukawa Dependence*, *JHEP* **01** (2014) 035 [[1310.4838](#)].

- [109] R. Alonso, E. E. Jenkins, A. V. Manohar and M. Trott, *Renormalization Group Evolution of the Standard Model Dimension Six Operators III: Gauge Coupling Dependence and Phenomenology*, *JHEP* **04** (2014) 159 [[1312.2014](#)].
- [110] A. Celis, J. Fuentes-Martin, A. Vicente and J. Virto, *DsixTools: The Standard Model Effective Field Theory Toolkit*, *Eur. Phys. J. C* **77** (2017) 405 [[1704.04504](#)].
- [111] J. Aebischer, J. Kumar and D. M. Straub, *Wilson: a Python package for the running and matching of Wilson coefficients above and below the electroweak scale*, *Eur. Phys. J. C* **78** (2018) 1026 [[1804.05033](#)].